frontiers in Earth Science

ORIGINAL RESEARCH
published: 20 April 2021
doi: 10.3389/feart.2021.637973

# Climate Patterns in the World's Longest History of Storm-Erosivity: The Arno River Basin, Italy, 1000–2019 CE

*Nazzareno Diodato*[1], *Fredrik Charpentier Ljungqvist*[2,3,4]* *and Gianni Bellocchi*[1,5]

[1]Met European Research Observatory—International Affiliates Program of the University Corporation for Atmospheric Research, Benevento, Italy, [2]Department of History, Stockholm University, Stockholm, Sweden, [3]Bolin Centre for Climate Research, Stockholm University, Stockholm, Sweden, [4]Swedish Collegium for Advanced Study, Linneanum, Uppsala, Sweden, [5]Université Clermont Auvergne, VetAgro Sup, INRAE, Clermont-Ferrand, France

Rainfall erosivity causes considerable environmental damage by driving soil loss. However, the long-term evolution of erosive forcing (over centennial to millennial time-scales) remains essentially unknown. Using a rainfall erosivity model ($REM_{ARB}$), this study simulates the variability of rainfall erosivity in Arno River Basin (ARB), Italy, a Mediterranean fluvial basin, for the period 1000–2019 CE resulting in the world's longest time-series of erosivity. The annual estimates show a noticeable and increasing variability of rainfall erosivity during the Little Ice Age (~1250–1849), especially after c. 1490, until the end of 18th century. During this cold period, erosive forcing reached ~1600 MJ mm $hm^{-2}$ $h^{-1}$ $yr^{-1}$ once every four years, and ~3000 MJ mm $hm^{-2}$ $h^{-1}$ $yr^{-1}$ once every 20 years. The extremes of rainfall erosivity (the 98th percentile) followed a similar increasing trend, with an acceleration of the hydrological hazard (erosivity per unit of rainfall) during the 20th century. The comparison of $REM_{ARB}$ output with the sediment yield of the basin (1951–2010) confirmed the model's ability to predict geomorphological effects in the ARB. Thus, our methodology could be applied to simulate erosivity in environmentally similar basins. A relationship has been identified between the Atlantic Multidecadal Variation and erosivity patterns, suggesting a role of North Atlantic circulation dynamics on the hydrology of central Italy's fluvial basins.

**Keywords: Arno river basin, erosivity density, historical dataset, increasing trend, parsimonious modeling, rainfall erosivity, reconstruction**

OPEN ACCESS

***Edited by:***
*Alexandre M. Ramos, University of Lisbon, Portugal*

***Reviewed by:***
*Pedro J. M. Costa, University of Coimbra, Portugal*
*Sérgio Oliveira, University of Lisbon, Portugal*

***Correspondence:**
*Fredrik Charpentier Ljungqvist*
*fredrik.c.l@historia.su.se*

***Specialty section:***
*This article was submitted to Atmospheric Science, a section of the journal Frontiers in Earth Science*

***Received:*** *04 December 2020*
***Accepted:*** *08 February 2021*
***Published:*** *20 April 2021*

***Citation:***
*Diodato N, Ljungqvist FC and Bellocchi G (2021) Climate Patterns in the World's Longest History of Storm-Erosivity: The Arno River Basin, Italy, 1000–2019 CE. Front. Earth Sci. 9:637973. doi: 10.3389/feart.2021.637973*

## INTRODUCTION

Damaging hydrological events triggered by either short and intense storms, or longer duration rainfall (e.g., Diodato et al., 2020b; Duulatov et al., 2021), cause sustained erosive forcing and considerable soil losses in many parts of the world (Wuepper et al., 2020). They may increase in frequency and/or severity with changes in the climate system associated with global warming (Easterling et al., 2000; Morera et al., 2017; Harris et al., 2018; Rineau et al., 2019; Wei et al., 2020). Understanding the dynamics and current developments of climate extremes (e.g., Garcia-Herrera et al., 2014) with rainfall erosivity pose significant challenges for quantifying their impact on landscapes. This is especially the case for Mediterranean environments (Diodato et al., 2011; Cramer et al., 2018) where autumn and early winter erosive storms cause significant floods and flash floods (e.g., Outeiro et al., 2010; Gascón et al., 2016; Diakakis, 2017). Existing studies on the interaction

between climate changes, hydrological regimes and water resources have hitherto raised a number of key questions for the hydrological community (Askew, 1991). They include the need to explore the mechanisms inherited from past hydrological events like storms, diluvial rains and floods, which cause damaging events (Hussain and Riede, 2020). Past climate changes reflect the changes occurring in the magnitude and intensity of surface processes (Thornes, 1990; Jongman, 2018; Sofia and Nikolopoulos, 2020) which, in turn, have influenced changes in the vegetation cover (Li et al., 2018) and recorded the imprint of human activities (Diffenbaugh and Field, 2013; Mueller et al., 2014). Floods have historically been a major natural hazard, and changed over time in frequency and/or severity, with prevailing climatic conditions (Brázdil et al., 2010; Glaser et al., 2010; Wetter et al., 2011; Rohr, 2013; Soens, 2013; Toonen, 2015; Kiss, 2019). In addition to climatic oscillations occurring at short hydrological intervals, medium-term changes and their long-term persistence can produce important hydrological extremes with geomorphological consequences (Viles and Goudie, 2003). In particular, climate variability and extremes at decadal and multi-decadal time-scales (Myhre et al., 2019; Boudet et al., 2020) can alter storm (rainfall) erosivity, i.e., the power of rainfall (that may cause soil erosion) represented by the R-factor of the Universal Soil Loss Equation (USLE) by Wischmeier and Smith (1978) and its revised—(R) USLE—versions (Brown and Foster, 1987; Renard and Freimund, 1994; Renard et al., 1997). Rainfall erosivity is important for understanding the dynamics of surface processes like soil degradation (Toy et al., 2002; Reimann et al., 2018) and other landscape stressors such as flooding and landslides (Schmidt et al., 2016). Its dynamics also offer the opportunity to possibly capture the fingerprint of recent climate change, particularly in the Mediterranean, which is considered a "hot-spot" of ongoing and future climate changes and a region particularly sensitive to climate variability on all time-scales (Zittis et al., 2019). In parts of the Mediterranean region, rainfall erosivity and, in turn, damaging hydrological events are often more disastrous and occurring more frequently than in the rest of Europe (Gaume et al., 2009; Llasat et al., 2010). They occur mainly because of: 1) intense, highly convective precipitation events of short duration (often less than 1 h) with limited total rainfall (usually less than 100 mm), and 2) mesoscale convective systems that produce stationary rainfall for several hours resulting in diffuse rainfall (the area of these events varies from several hundred to several thousand km$^2$) of more than 200 mm in a few hours (Gaume et al., 2018). Then, mixtures of convective and mesoscale systems can produce changes of rainfall systems and thus contribute to erosive storms irregularly distributed in this region (Diodato and Bellocchi, 2012).

The current trend toward more extreme precipitation events in the Mediterranean region is expected to continue over the coming decades, making uncertain the future projection of damaging hydrological events (Lenderink and Fowler, 2017). In this context, a better understanding of temporal changes in erosive rainfall (and the correlated landscape damages) has important implication for the implementation of conservation and environmental management plans (De Luca and Galasso, 2018). Recent studies about the relationship between hydrological extremes and climate (Corella et al., 2016; Zscheischler et al., 2020), agriculture and flooding (Kaniewski et al., 2016; Tabari, 2020), sediment connectivity (Sofia and Nikolopoulos, 2020), water quality (Puczko and Jekatierynczuk-Rudczyk, 2020) and biological processes (Harris et al., 2020) indicate a renewed attention by environmental scientists to the history of extreme climatic events. Our still limited understanding of past hydroclimatic dynamics and extremes undermines the ability to generate plausible predictions about future fluvial flooding (Zhang et al., 2017). The inability of most early instrumental station records and, even more so, documentary-based or natural proxy-based paleoclimate reconstructions to capture high-frequency extreme events has obviously limited the ability to place anthropogenic climate change in relation to overall long-term natural variability across different time-scales. In fact, although the mean climate and rates of change may still be within the range of natural variability, changes in magnitude or the return time of some climate extremes may not be. However, some knowledge may be drawn from historical documentary data. Leonardo da Vinci (1452–1519) documented his hydrological observations in the Trattato sull'acqua ("Treatise on water"), published in 1489, which enrich in many details the representation of the landscape and the aggressiveness of storms and river floods in the Mediterranean region (Pelucani et al., 2017, p. 202):

> *Vedeasi le antiche piante diradicate e stracinate dal furor de' venti vedevasi le ruine de' monti, già scalzati dal corso de' lor fiumi, ruinare sopra e medesimi fiumi e chiudere le loro valli li quali fiumi ringorgati allagavano e sommergevano le moltissime terre colli lor popoli*
>
> You could see the ancient plants uprooted and overgrown by the fury of the winds; you could see the ruins of the mountains, already undermined by the course of their rivers, ruin over the same rivers and close their valleys; which rivers, when they were surrounded, flooded and submerged the many lands with their people

Furthermore, Leonardo, in Trattato della natura, peso e moto delle acque, e osservazioni sul corso de' fiumi ("Treatise on the nature, weight and motion of the waters and observations on the course of the rivers") continues with (Cardinali, 1828, p. 395):

> *Devesi per le piogge, o veramente avendo comodità d'altr'acqua fare passare canali, o bocche di fiumi per li luoghi e terreni, donde passion con gran corso in modo, che s'abbino a intorbidare dalla terra che levano, ed adattare in modo, che quando essi sono alli luoghi dove tu vuoi che ivi scaricano detta terra*
>
> When it rains, or when it is convenient to have other water, channels or mouths of rivers must be made to pass through the places and lands from which they flow with a great course, so that they may be clouded by the earth they raise, and so that when they reach the places where you want them to discharge the said earth there

Leonardo formulated some of the first scientifically-sound theories of hydrological variability by documenting the flooding of the Arno River Basin (ARB) in the Tuscany region of central Italy (Pfister et al., 2009), which is the focus of this study. The Italian territory is mostly exposed to aggressive rains (**Figure 1A**) and, within Italy, the ARB is even more exposed than

other areas (**Figure 1B**). Here, high-intensity rainfall can occur in any month due to the occurrence of thunderstorms throughout the year, which in turn provide considerable rainfall erosivity values (~700–4000 MJ mm $hm^{-2}$ $h^{-1}$ $yr^{-1}$ over the 2003–2012 period, **Figure 1B**).

If we consider the recent past, there are also great and effective examples of studies on the trend of erosive phenomena in the central Mediterranean region (Capolongo et al., 2008; Grauso et al., 2010; Cevasco et al., 2015; Diodato et al., 2016; Capra et al., 2017; Acquaotta et al., 2019). With some exceptions where the reconstruction of erosive trends date back to the 16th or 17th century (Diodato et al., 2008; Diodato et al., 2020a, b) these works have only made it possible to estimate rainfall erosivity for recent decades. The Florentine landscape, as we know it today, has developed since the 11th century, with its agricultural and urban activities, and is an example of the hilly and mountainous landscapes characterizing the central Mediterranean region, where changes in climate and its extremes intertwine with the life of local communities. During medieval times, the growth of Florence extended on both banks of the Arno (Salvestrini et al., 2010). The economic and social life of the city gradually evolved in contact with the river, from which Florence had to protect itself (**Figure 2A**). Sometimes, during the extraordinary floods that occurred from time to time, the walls to protect the city from the water were not enough, and then the Arno leaned on the city in some places, or entered it as during the flood of 1844 (**Figure 2B**). The Arno River Basin has a markedly torrential morphological nature. There is no recorded memory of particularly disastrous floods in the area of ancient Florentia during Antiquity (roughly between the 8th century BCE and the 6th century CE). The scarce presence of settlements along the banks of the river, as well as the existence of the Bisarno river (a variant of the Arno river bed facilitating water outflow) to the north-east of the city, meant that autumn or spring floods did not cause noteworthy damage (Morozzi, 1766). In the centuries following the year 1000 CE, the Arno Basin has been subject to frequent flooding, which has affected in particular the areas near the river and its most important tributaries, as well as the marshy areas that dotted the bottom of the valley, which are large reservoirs to collect the flood waters (Salvestrini et al., 2010). At that time Tuscany was subject to extreme events and erosive rains, which took place, with different frequency, throughout the second millennium CE, when the region was exposed to deforestation-related hydrological risks (Andreolli and Montanari, 1988; Hofman and Perulli, 2000).

In this study, we address the long-term estimation of annual rainfall erosivity in the ARB. According to the Revised Universal Soil Loss Equation—(R)USLE—methodology (Renard et al., 1997), the rainfall erosivity factor ($R$) is calculated through an empirical relationship of precipitation intensities measured during 30 min ($R = E{\cdot}I_{30}$). For a given site or area, the monthly $R$ values ($R_m$) are the sum of all $EI_{30}$ values of single storms for that month. The term $EI_{30}$ (MJ mm $h^{-1}$ $hm^{-2}$) is the product of the kinetic energy of the storm ($E$), calculated in time steps of a few minutes of constant storm intensity, and the maximum intensity in 30 min ($I_{30}$). Such measurements are generally not available before the modern instrumental period (digital measurements first systematically began in the 1980s; Diodato, 2004), and the only possibility to obtain past rainfall erosivity data is that offered by parsimonious modeling approaches, which use proxy (indirect) inputs from long-term storms and floods (Diodato et al., 2017a). Modeling approaches using low-resolution precipitation data—both temporal (annual or finer resolution) and spatial (not locally calibrated, Poirier et al., 2016)—and documentary records of extreme weather events allow for long-term reconstructions (Diodato et al., 2008). To assess the historical documentary data about the damaging hydrological events that occurred in the ARB over the 1000–2019 CE period, we have used meteorological anomalies such as storms and floods, and their variability. In particular, we aimed at 1) developing a parsimonious model to reconstruct annual rainfall erosivity during the period 1000–2019 CE, and 2) capturing a wide range of climate variability and, in turn, identifying changes in landscape stress.

# MATERIALS AND METHODS

## Study Area and Climate

Arno is the second most important river of central Italy (241 km long). It originates on Mount Falterona at 1385 m a.s.l. and flows into the Tyrrhenian Sea at Marina di Pisa (43°40′N, 10°16′E). The river flooded Florence quite often in historical times, most recently in 1966 (November 4), with 4500 $m^3$ $s^{-1}$ after rainfall of 437.2 mm in Badia Agnano (43°26′N, 11°38′E, 271 m a.s.l.) and 190 mm in Florence, in 24 h (Martin, 1967). Located across the northern Apennine chain (**Figure 3**), the Arno River Basin (ARB), from its origin to the outlet, has an area of ~8229 $km^2$, with an average elevation of ~353 m a.s.l. The Casentino forest massif, in the province of Arezzo (43°28′N, 11°52′E, 134–954 m a.s.l.), is the valley in which the first tract of the Arno River flows. Then, it enters the upper Valdarno (highlighted in **Figure 3**), a long valley bordered on the east by the Pratomagno massif and on the west by the hills around Siena (43°19′N, 11°19′E, 200–510 m a.s.l.).

In the middle and lower Valdarno, the course of the Arno forms an important natural demarcation between the areas north of the river, which are cooler and rainier, and those south, which are warmer and more arid. The climate of the ARB is determined by its position in relation to the direction of wind motion (with an intense western disturbance) and geographical factors such as distance from the sea, and elevation, orientation and distribution of the reliefs, which determine a marked differentiation of climates. The highest mean annual precipitation values, >1500 mm, occur on the crests of Pratomagno and the upper Casentino. The Arno receives water from several tributaries. From the right side, the river Sieve comes from Mugello reliefs (43°95′N, 11°38′E, 162–437 m a.s.l.), while in the southern part of the basin (Val di Chiana, 43°15′N, 11°49′E, 405 m a.s.l. on average), the rivers Pesa and Era form the valleys of the left-side sub-basins. Here, annual precipitation varies between 800 and 900 mm. Rainfall intensity >100 mm $d^{-1}$ occurs in most of the basin, with peaks of 180–200 mm $d^{-1}$ in some sectors of the Apennines (Monti and Rapetti, 2011).

## (R)USLE-Based Actual Rainfall Erosivity Data

Annual (R)USLE-based erosivity data were obtained for 1964–1990. This calibration period covers two climatic regimes, with a temperature decrease and weak winter westerlies until about 1976, and a strong temperature increase and winter westerlies after about 1976 (Mariani and Diodato, 2014). The actual erosivity data were obtained from Bazzoffi and Pellegrini (1990) at Vicarello di Volterra and Cevasco et al. (2015) at Levanto, and derived from Borselli et al. (2004) and Angeli et al. (2007) at Florence based on a power relationship between the R-factor and the monthly rainfall data (source: SCIA—National System for Climate Data Collection and Dissemination, http://www.scia.isprambiente.it). With about 2300 (Levanto), 1718 (Florence) and 731 (Vicarello di Volterra) MJ mm $hm^{-2}$ $h^{-1}$ $yr^{-1}$ on average, the three sites (**Figure 1C**, red circles) are representative of situations occurring in three sectors of the ARB. Located on the Ligurian coast (north-western Mediterranean) and at the foothills of Tuscany, Levanto is representative of hydrological conditions occurring in upper Valdarno, characterized by heavy precipitation events leading to large amounts of rainfall (Hofstätter et al., 2016). Florence is located in the southwest corner of the middle Valdarno, marked by annual precipitation totals of 800–900 mm. Vicarello di Volterra is located downstream of Florence, in the lower Valdarno, a broad valley where the average annual rainfall is below 800 mm. The weighted areal mean of actual rainfall erosivity (MJ mm $hm^{-2}$ $h^{-1}$ $yr^{-1}$) for the Arno Basin (*RS*) was calculated for each year of the period 1964–1990 as a linear combination of the site-specific erosivity values ($S_1$: Levanto; $S_2$: Florence; $S_3$: Vicarello di Valdarno):

$$RS = s \cdot (a_1 \cdot S_1 + a_2 \cdot S_2 + a_3 \cdot S_3) \quad (1)$$

where one scale factor $s = 1.35$ and three relative weighting factors $a_1 = 0.2$, $a_2 = 0.1$ and $a_3 = 0.7$ are calibrated values to converge to the long-term areal mean (1541 MJ mm $hm^{-2}$ $h^{-1}$ $yr^{-1}$; **Figure 1B**). The estimated scale factor $1 < s < 2$ is an upscaling parameter, which is consistent with the assumption that individual sites are fractal elements of the area (e.g., Diodato et al., 2017b). The estimated relative weighting factors $a_i$ ($i = 1, 2, 3$) reflect the characteristics of the three stations (e.g., Bartolini et al., 2018). At the low end of the ARB, Vicarello di Volterra (station $S_3$) has the greatest influence on the areal erosivity because it is located upwind of the western currents that are the bearers of heavy rainfall. As they advance eastward and northeastward, many of these storms transfer energy in the form of erosive rain over much of the basin. Outside the basin, Levanto (station $S_1$) also maintains an upwind position with respect to the northern Apennine slopes, but thunderstorms are forced to move east and northeast, thus passing only over some areas of the river basin. Finally, Florence (station $S_2$) contributes the least as it is located far from the sea and is not much affected, on average, from the heaviest rainfall that discharges its energy before reaching the easternmost part of the basin.

We used **Eq. 2** to reconstruct a time-series of annual storm erosivity (MJ mm $hm^{-2}$ $h^{-1}$ $yr^{-1}$) in the ARB from 1000 to 2019 CE. We also obtained erosivity density—**Eq. 3**—using the rainfall (mm) data provided for the period 1891–2016 (~900 mm on average) by the GPCC (Global Precipitation Climatology Center) by 0.25° monthly land-surface precipitation dataset Schneider et al. (2018), built on global telecommunication system-based and historical data (https://opendata.dwd.de/climate_environment/GPCC/html/fulldata-monthly_v2018_doi_download.html).

## Numerical and Categorical Inputs

In addition to extensive research in the main Italian historical archives and libraries, literary sources were consulted by web search (https://books.google.com), which generated ~100,000 bibliographical documents. We collected a massive bibliographic dataset but only ~500 records have met the criteria of including the keywords abundant rainfall, storm, downpour, diluvial, flood and alluvial (*piogge abbondanti, tempesta, nubifragio, diluvio, inondazione, alluvione*), as well as some Latin locutions (e.g., *magnae pluviae, aqua maxima, diluvium, excrescentia fluminum, inundatio*) that were chosen for careful reading. Useful data were extracted from documentary sources by converting the information contained in historical accounts (Morozzi, 1766; Aiazzi, 1845; Giorgini, 1854; Rossini, 1855; Becchi and Paris, 1989; Salvestrini, 2005; Menduni, 2017; Pelucani et al., 2017; Ricci et al., 2017; Rombai et al., 2017; Salvestrini et al., 2017) into numerical values on an index scale (see **Supplementary Material S1**—erosivity reconstruction in **Supplementary Material**). Transformation process required a dynamic understanding of the historical information used in the analysis, with an in-depth knowledge of regional and sub-regional climates, and familiarity with the relative strengths and weaknesses of each type of source. Weather hind-casting (Pfister et al., 2018) was used to familiarize with well-documented anomalies in the instrumental period before analyzing similar cases in the pre-instrumental time. Storms occurring during the summer season (May to August) were not considered in this study, as they generally only affect small or isolated areas of the ARB and are not representative for long-term storm reconstruction. A scoring system was thus established (Wetter et al., 2011) to rate the MSSI (defined in the time of year between September and April) as 0 (normal), 1 (stormy), 2 (stormy with some flooding), 3 (stormy with important flooding), and 4 (extraordinarily stormy with major flooding):

Normal: average storm or storm passed unobserved, without comments about its severity or its impacts on society and economy.

Stormy: intense rainfall occurred with only limited damage, and no floods recorded.

Very stormy: intense rainfall occurred with some floods.

Great stormy: extreme diluvial event, with severe and large floods, agricultural works suspended, and urban communications interrupted.

Extraordinary stormy sporadic, very extreme event, with a centennial recurrence rate (these extreme diluvial events affect several river basins at the same time, killing people and animals, and felling trees).

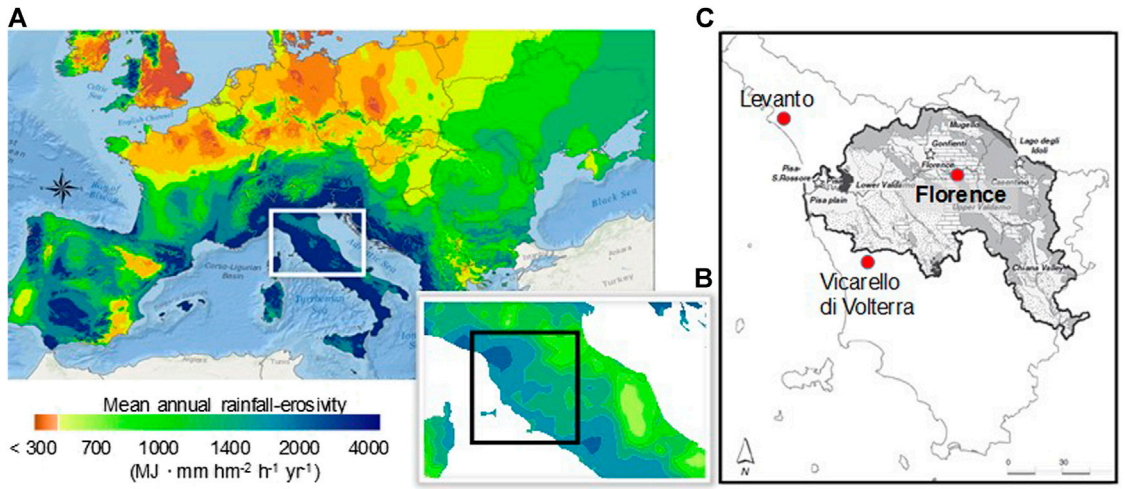


**FIGURE 1 |** Study area and environmental setting. **(A)** Spatial pattern of mean annual rainfall erosivity over central-southern Europe in the period 1994–2013 (using Geostatistical Analytics by ArcGIS-ESRI on the European Soil Data Centre-dataset, https://esdac.jrc.ec.europa.eu/content/global-rainfall-erosivity, Panagos et al., 2015), **(B)** as **(A)** with focus on the Tuscany region (black square), and **(C)** Arno River Basin (in gray) with the pluviometric stations (red dots) providing the actual rainfall erosivity data used (following Benvenuti et al., 2011): Vicarello di Volterra (43°24′N, 10°52′ E, 531 m a.s.l.), Levanto (44°10′N, 09°36′E, 3 m a.s.l.), Florence (43°47′N, 10°15′E, 50 m a.s.l.).

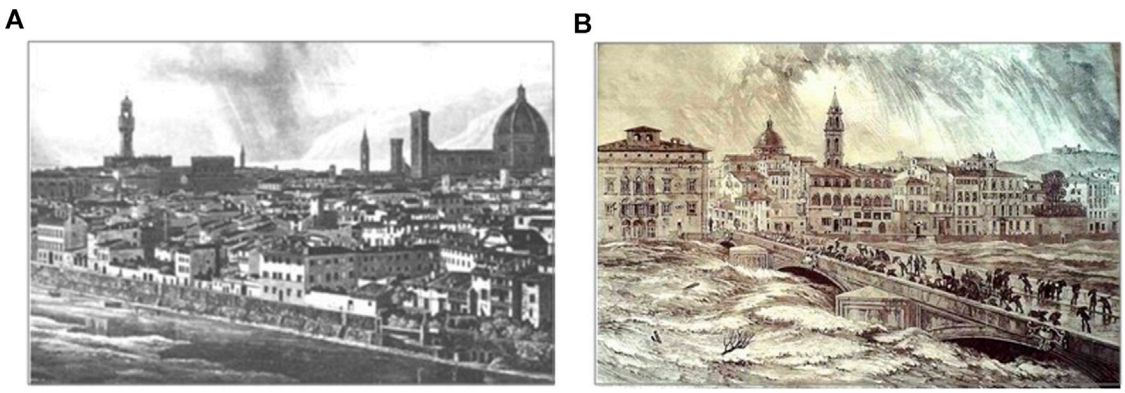


**FIGURE 2 |** Overview of Florence landscape under diluvial storms. **(A)** Arno, near the city of Florence, in its original configuration (as presented by Menduni, 2017) dating back to 1287, in an engraving made shortly before the work for Florence enlargement designed by Giuseppe Poggi (1811–1901), and **(B)** the flood of the river on November 4, 1844 (from https://www.conoscifirenze.it/libri-free-su-firenze/335-Inondazioni-in-Firenze-1844-1864.html).

The study was based on the systematic and critical analysis of data on the above phenomena provided by Italian documentary sources. For most of the information, it was possible to carry out an "event check" considering more than one documentary source on the same event. It was also possible to contextualize the storms with other types of historical events (e.g., social, agricultural, religious). In this way, the reliability of information was assessed going beyond quantitative data and looking for other sources of information such as diaries, newspapers, chronicles and local stories.

## Rainfall Erosivity Model

For the historical reconstruction of annual rainfall erosivity (MJ mm $hm^{-2}$ $h^{-1}$ $yr^{-1}$) in the ARB, we developed the Rainfall Erosivity Model for the Arno River Basin ($REM_{ARB}$), which combines low-resolution explanatory inputs to form a parsimonious concept compatible with the scenario depicted by (R)USLE-based erosivity data (Renard et al., 1997). The non-linear model of annual erosivity in the ARB takes the following form:

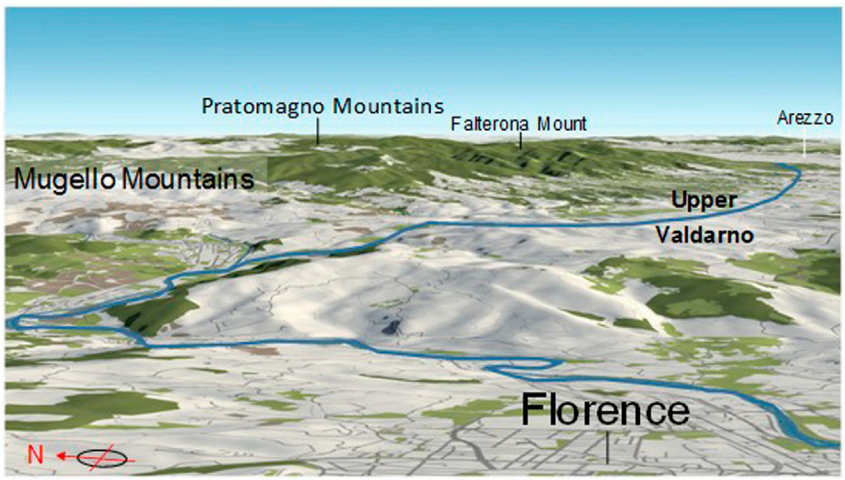


**FIGURE 3 |** Perspective view of Arno River Basin from the east. The highest elevations are found on the Mount Falterona (43°52′N, 11°42′E, 1654 m a.s.l.) and the mountainous group of Pratomagno, where they reach 1658 m a.s.l. on Monte Falco (43°52′N, 11°42′E), 1592 m a.s.l. on Croce di Pratomagno (43°39′N, 11°39′E) and 1537 m a.s.l. on Poggio Uomo di Sasso (43°41′N, 11°37′E). The Arno river winds through the landscape, passing through the city of Florence after leaving its source. With a length of 241 km, it crosses Florence (43°47′N, 10°15′E, 50 m a.s.l.). Map is an output image created from OpenStreet Map (https://tinyurl.com/y4qa79fu).

$$REM_{\mathrm{ARB}} = A \cdot \left[\alpha + \left(\sum_{i \in X} \mathrm{MSSI_i}\right)^{k}\right] + B \cdot \left[\beta + SD_{i \in Y}\left(\mathrm{MSSI_i}\right)^{k}\right] \cdot \left(\gamma + \sum_{i \in Z} \mathrm{MSSI_i}\right) \quad (2)$$

where: $A$ (MJ mm$^{-1}$ hm$^{-2}$ h$^{-1}$ yr$^{-1}$) and $B$ (MJ mm$^{-1}$ hm$^{-2}$ h$^{-1}$ yr$^{-1}$) are scale parameters converting the result of two dimensionless terms of the model into the output unit; α, $\beta$ and $\gamma$ are shift parameters estimating rainfall erosivity when the monthly input values ($i$ = 1, . . ., 12 months) of the storm-severity index ($\mathrm{MSSI_i}$) are all equal to zero; $k$ is a shape parameter; SD is standard deviation; X ($i$ = 9, 10, 11), Y ($i$ = 1, 2, 3, 4, 9, 10, 11, 12) and Z ($i$ = 1, 2, 3, 4, 12) are different groups of months (where the symbol $\in$ stands for "belongs to"). The erosivity model was designed not to contain a position parameter, i.e., a constant term prescribing the fixed amount that contributes to rainfall erosivity when all other terms of the equation are equal to zero. In this way, the model predicts a null rainfall erosivity for null input values.

The concept of the model is summarized in **Figure 4**. Complex climatic characteristics affect erosive rainfall, depending on rain-splash, runoff and flood generation mechanisms, and it is difficult to disentangle the climatic component from substantial natural variability and anthropogenic impacts (Sofia and Nikolopoulos, 2020). According to Waldman (2010) and Diodato and Bellocchi (2014), non-linear relationships emerging across river basins depend on the processes that dominate a given hydrological regime.

In southern Europe, erosive storms mostly occur in autumn, when the occurrence of severe thunderstorms is intimately associated with convective processes (e.g., Guzzetti et al., 2003; Diodato and Bellocchi, 2012; Petrucci et al., 2014; Ballabio et al., 2017). Spring precipitation likely leads to a different regime of hydrological extremes compared to September–October, when extreme floods are more frequent. This indicates that the period September–April delineates a key time-window in the year for estimating rainfall erosivity in fluvial basins. The separation between advective and convective events is considered important, assuming that convective precipitation (short and intense) has a greater dynamic and variability than generally more static advective events.

The seasonal differences in precipitation are governed by convective processes, more dynamic and frequent in summer (when rain-splashes dominate), or by a variable mixture of convective and advective precipitation, more frequent in autumn (when overland flows dominate). Then, winter and spring rainfall (long-lasting and low-intensity), which usually originates from broad frontal activity, carries large volumes of rainwater (through orographic stratiform precipitation) that cause large-scale hydrological processes like flooding (Van Delden, 2001). These processes are mostly captured in the $REM_{\mathrm{ARB}}$—**Eq. 2**—by MSSI. Very intense convective events, or those of a mixed advective-convective nature (with high kinetic energy causing local showers and leading to splash-erosivity processes) are interpreted by the SD term. The erosivity density (ED, MJ hm$^{-2}$ h$^{-1}$) in the ARB ($ED_{\mathrm{ARB}}$) was calculated for the 1891–2016 period as:

$$ED_{\mathrm{ARB}} = \frac{REM_{\mathrm{ARB}}}{P_{\mathrm{ARB}}} \quad (3)$$

where $P_{\mathrm{ARB}}$ (mm yr$^{-1}$) is the annual precipitation in the basin.

## Model Calibration and Assessment

To assess the model, statistical analyses were performed with STATGRAPHICS (http://www.duke.edu/~rnau/sgwin5.pdf), with the graphical support of WESSA (https://www.wessa.net)

and AgriMetSoft Online Calculators (https://agrimetsoft.com/calculatorshttps://www.curveexpert.net/). The parameters of **Eq. 2** were calibrated against actual rainfall erosivity data according to statistical criteria. The first condition was to minimize the distance between modeled and actual erosivity data, by minimizing the Mean Absolute Error (optimum, $0 \leq \text{MAE} < \infty$, MJ mm $\text{hm}^{-2}\,\text{h}^{-1}\,\text{yr}^{-1}$). Complementary to the MAE, the MAPE (mean absolute percent error) offers the advantage of being scale-independent and intuitive (e.g., the prediction model is considered reasonable with a MAPE below 30% and very accurate with a MAPE less than 10%). The second condition is to maximize the determination coefficient ($0 \leq R^2 \leq 1$, optimum) that is the variance explained by the model. The third conditions approximates the unit slope of the straight line that would minimize the bias of the linear regression actual vs. modeled data (b = 1, optimum). In addition, the Kling-Gupta index ($-\infty < \text{KGE} \leq 1$) was used as efficiency measure, with KGE>–0.41 indicating that a model improves upon the means of observations as a benchmark predictor. The Nash-Sutcliffe efficiency index ($-\infty < \text{EF} \leq 1$, optimum; Nash and Sutcliffe, 1970) has also been calculated as an indicator of model performance uncertainty because values above 0.6 indicate limited model uncertainty, presumably associated with narrow parameter uncertainty (Lim et al., 2006). To select the set of important covariates for the parsimonious model for estimating actual erosivity data, we iteratively added in predictors, one-at-a-time until modeling solutions with small MAE and large $R^2$ values were obtained. Then, for the final selection, a third criterion $-|b-1| = \min -$ was additionally involved. Each predictor was repositioned over >50 iterations until convergence was achieved. The Durbin-Watson statistic was performed to test for auto-correlated residuals because large temporal dependence may induce spurious correlations. ANOVA *p*-values were used to present the statistical significance of the regression between estimates and the actual observation-based data.

# RESULTS AND DISCUSSION

## Completeness of the Reconstructed Extreme Hydrological Events

We have extracted 369 extreme hydrological events, occurring in the ARB from 1000 to 2019 CE. The classification of these events by severity led to 213 stormy events, 98 very stormy events, 41 great stormy events, and 17 extraordinary stormy events. However, our historical hydrological database is based on several types of heterogeneous sources, including reports that may be an exaggeration of what was an uncritical reference to previous sources, printing errors in the documentation, and natural records of environmental factors ("proxy" data). All of them contain different sources of uncertainty in the "cataloguing" of storm records (Pavese et al., 1994). It is well ascertained, for instance, that small storms tend to be underestimated, especially those far from inhabited centers, while more localized ones can be frequent. In order to resolve some of these uncertainties in our database, we have established a reasonable standard for Monthly Storm-Severity Index (MSSI) recorded events. This was facilitated by defining a partition of the time-series in three equally-long sub-periods following Diodato et al. (2019b),—1000–1340 (**Figure 5A**), 1341–1680 (**Figure 5B**), and 1681–2019 (**Figure 5C**)—and verifying, for each sub-period and for the entire dataset (**Figure 5D**), the scale-invariance in the relationship between the number of events larger than the strength of a given storm event and the same strength event. The completeness analysis was formalized with the relationship between the cumulative number of events (*CEN*) and the MSSI values in the range $1 \leq \text{MSSI} \leq 4$, as follows:

$$\log_{10}\left(CEN_{i,j}\right) = a + b \cdot \text{MSSI}_{i,j} \text{ with } i = 1, \ldots, 4 \text{ and } j = 1, \ldots, 4 \quad (4)$$

where MSSI is the Monthly Storm-Severity Index by severity class (*i*) and sub-period (*j*). In total, 369 events within the range $1 \leq \text{MSSI} \leq 4$ are described in qualitative terms as stormy, very stormy, great stormy and extraordinary stormy.

The negative slopes in the three sub-periods, and for the entire dataset, reflect the principle of a progression toward a lower frequency as storms become more severe. With determination coefficients $0.97 \leq R^2 \leq 1.00$, it can be assumed that storms in the period 1000–2019 CE are scale-invariant and that ancient sources from different periods are not too fragmentarily available to facilitate a quantitative reconstruction (Mazzarella and Diodato, 2002).

## Rainfall Erosivity Model Calibration and Validation

To estimate the annual values of the mean rainfall erosivity in the ARB, we developed and calibrated a simplified statistical model ($REM_{\text{ARB}}$)—**Eq. 2**—which summarizes (through MSSI inputs) the relationship between spatial patterns of climate and storm erosivity, consistent with a sample (1964–1990) of detailed (R) USLE-based data obtained for the study area with **Eq. 1**. The mean actual erosivity is 1541 MJ mm $\text{hm}^{-2}\,\text{h}^{-1}\,\text{yr}^{-1}$ (±340 standard deviation), the values varying between 1134 (in 1977) and 2306 (in 1981) MJ mm $\text{hm}^{-2}\,\text{h}^{-1}\,\text{yr}^{-1}$. In the same period (1964–1990), the calibrated model gave 1542 MJ mm $\text{hm}^{-2}\,\text{h}^{-1}\,\text{yr}^{-1}$ on average (±340 standard deviation), and 1256 (in 1977) and 2487 (in 1966) MJ mm $\text{hm}^{-2}\,\text{h}^{-1}\,\text{yr}^{-1}$ as minimum and maximum estimates, respectively. A qualitative validation for the 1951–2010 period was also introduced in order to control if modeled rainfall erosivity can be representative of the erosional sediment processes that happen across the ARB. For the calibration period 1964–1990, we obtained the coefficients $A = 58.85$ MJ $\text{mm}^{-1}\,\text{hm}^{-2}\,\text{h}^{-1}\,\text{yr}^{-1}$, $B = 1.00$ MJ $\text{mm}^{-1}\,\text{hm}^{-2}\,\text{h}^{-1}\,\text{yr}^{-1}$, $\alpha = 10.00$, $\beta = 4.61$, $\gamma = 2.46$ and $k = 2.00$ in **Eq. 2**. With these values, the linear regression between actual and estimated erosivity data is statistically significant (F test $p$~0.00). The $R^2$ statistic (goodness of fit) indicates that the $REM_{\text{ARB}}$ explains 88% of the erosivity variability. MAE (mean absolute error) equal to 96 MJ mm $\text{hm}^{-2}\,\text{h}^{-1}\,\text{yr}^{-1}$ and MAPE (mean absolute percent error) equal to 7%, with Kling-Gupta Efficiency (KGE) equal to 0.91, indicate satisfactory model performance and efficiency.

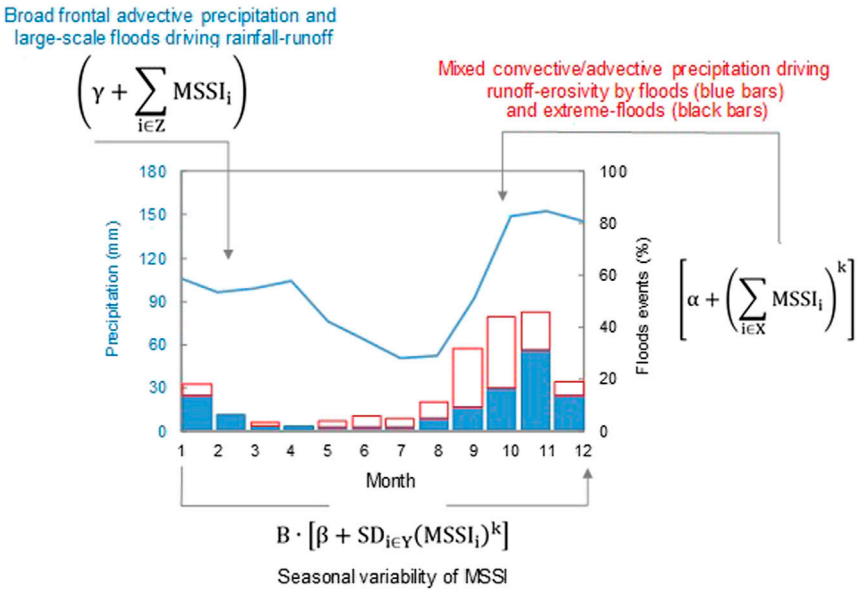


**FIGURE 4 |** Monthly precipitation and frequency of floods and extreme floods (1940–2015) over the Arno River Basin. Monthly rainfall totals (blue line) are from GPCC (Global Precipitation Climatology Center) by 0.25° monthly land-surface precipitation dataset (Schneider et al., 2018). Percentages of monthly floods (white, red-contoured bars) and extreme floods (blue, red-contoured bars) are from this study and Gaume et al. (2018), respectively. The terms of **Eq. 2** are reported.

Although there is an indication of possible serial correlation in the residuals (Durbin-Watson statistic $p < 0.05$), the calibrated regression (**Figure 6A**, black dotted line) shows only negligible departures of data-points from the 1:1 identity line (red line), which indicates the substantial ability of the model, **Eq. 2**, to predict actual erosivity. In fact, the Nash-Sutcliffe efficiency value (EF = 0.88) indicates limited uncertainty in model estimates. In particular, the regression line has an intercept a = −0.58 (±114.4) MJ mm $hm^{-2}$ $h^{-1}$ $yr^{-1}$ and a slope b = 1.00 (±0.1) near or equal to the optimum values (a = 0 and b = 1). **Figure 6B** indicates the normal approximation of model residuals (normality test $p > 0.05$, Jarque and Bera, 1981). The distribution of the percentiles of modeled rainfall erosivity (**Figure 6C**, orange curve) approaches the distributional shape of the observed erosivity, indicating a satisfactory prediction over the range of erosivity values (including the low and high erosivity values).

Di poi le molte pioggie, accrescimento dei fiumi, con ispessi lavamenti à dispogliati in parte l'alte cime d'essi monti, lasciando il loco della terra, il sasso si trova essere circondato dall'aria, e la terra d'essi lochi partita

The qualitative validation shows that modeled erosivity can be a representative driver of erosional sediment processes occurring in the ARB (**Figure 6D**). The interannual variation in the volumes of soil potentially transported through the ARB shows an overall downward trend, although with some large fluctuations, and this is sufficiently described by our modeled erosivity. Some discrepancies between the two lines could be due to inaccurate determinations of the transport of sand in the Arno river bed, in particular for the year 1960, for which no extreme rainfall was detected in any of the ARB pluviometric station. According to Monti and Rapetti (2011), the extraction of large volumes of inert materials can be associated with an intense potential transport, concentrated between the late 1950s and the first half of the 1960s. We have confirmation that pluviometric events (not soil and landscape features) are the main forcing agent of sediment from authors' own words (Monti and Rapetti, 2011, p. 124):

> *I risultati della ricerca dimostrano che il F. Arno e il suo bacino, in presenza di eventi pluviometrici estesi e prolungati, nonostante le modificazioni che hanno interessato l'unità fisiografica, conservano la capacità di sviluppare elevate portate liquide e rilevanti trasporti potenziali di sabbie sul fondo*
>
> The results of the research show that the Arno river and its basin, in the presence of extensive and prolonged rainfall events, despite the changes that have affected the physiographic unit, retain the ability to develop high liquid flows and significant potential transport of sand on the bottom

This analysis then points out that the baseline categorical MSSI was a reliable substitute of storm rainfall.

## Historical Rainfall Erosivity Reconstruction

**Figure 7A** shows the evolution of the estimated annual rainfall erosivity values (blue circles) obtained by **Eq. 2** for the ARB (areal mean) over the 1,000–2019 CE period: mean 1,412 (±393 standard deviation), minmum 1256, maximum 4892 MJ mm $hm^{-2}$ $h^{-1}$ $yr^{-1}$. The distributional properties of the actual data sample and the millennium-long reconstructed time-series are more similar as moving toward the highest percentiles (data not shown). An issue is how to develop a continuous time-series of the annual output when integer monthly inputs are present. In our case, the use of integer values for the MSSI may not sufficiently reflect the fluctuations that occur in the annual rainfall erosivity. For a better identification of possible trends and

oscillations in the estimated data and compare contemporary and historical patterns, the time-series of annual rainfall erosivity was also filtered using a 11-years low-pass Gaussian function (**Figure 7A**, bold blue curve). We observe that the world's longest series of annual erosive rainfall, dating back to the latter half of the Medieval Climate Anomaly (MCA; here 1000–1249 CE), is associated with frequent low-erosivity storms (~1300 MJ mm $hm^{-2}$ $h^{-1}$ $yr^{-1}$), which occurred once every four years. During the MCA, infrequent extreme erosivity values (~2000 MJ mm $hm^{-2}$ $h^{-1}$ $yr^{-1}$) were only present in ~3% of the years (i.e., in 1011, 1029, 1050, 1060, 1080, 1086, 1117, 1050, 1129, 1139, 1272, 1282 and 1333), while the years 1168 and 1179 are exceptional, with ~4000 MJ mm $hm^{-2}$ $h^{-1}$ $yr^{-1}$. For these years, the 12th-century chronicler Bernardo Maragone reported nine and 13 floods, respectively (Salvestrini et al., 2017). This long-term erosivity pattern is similar to that found by Longman et al. (2019) for the eastern Mediterranean region, reflecting less rainy conditions with limited hydroclimatic variability during much of the MCA. With the onset of the Little Ice Age (LIA; here 1,250–1849 CE), erosivity often became more vivid (likely associated with the enhanced variability of dynamical processes, e.g., Raible et al., 2018), with values mostly just below 2000 MJ mm $hm^{-2}$ $h^{-1}$ $yr^{-1}$ (corresponding to the 95th percentile of the whole series, yellow line in **Figure 7A**). These natural events had disastrous consequences in much of western Europe (Pouzet and Maanan, 2020). The second decade of the 14th century was affected by exceptionally high rainfall in Atlantic Europe, which had "water at ankles" level, according to the iconic formula of Le Roy Ladurie (1982). Taking special care in describing damaging hydrological phenomena over the 14th century, the chroniclers' texts convey useful information not only to know the climate of that century but also the characteristics of climate impacts on society, agriculture and transport, and the measures taken to protect the territory surrounding the river and the town of Florence. Giovanni Villani (c. 1280–1348) reports the catastrophic flooding associated with the erosive event of 1333 (estimated value equal to 2509 MJ mm $hm^{-2}$ $h^{-1}$ $yr^{-1}$), whose chronicle is an example of the importance of the narrative form used in historical accounts (as from the posthumous work Villani, 1587, p. 673): ... *per lo modo che chi lo leggerà per lo tempo avvenire, potrà comprendere i termini fermi e notabili onde faremo menzione appresso* ("... for the way that those who will read it for the time to come, will be able to understand the firm and notable terms that we will mention below").

That exceptional event was the result of a more general regional-scale shift, which can be considered the main cause of the hydrological change that occurred during that period, also in other areas of northern Italy (Glur et al., 2013; Baldini and Bedeschi, 2018; Diodato et al., 2020c). Leonardo da Vinci himself, who knew the territory of Tuscany well, left many drawings with projects that were supposed to alleviate the effects of the increasingly dangerous floods and soil erosion (Pelucani.et al., 2017). On sheet 126 v. of the *Codex Atlanticus* Leonardo writes (De Lorenzo, 1871, p. 122):

> *Di poi le molte pioggie, accrescimento dei fiumi, con ispessi lavamenti à dispogliati in parte l'alte cime d'essi monti, lasciando il loco della terra, il sasso si trova essere circondato dall'aria, e la terra d'essi lochi partita*
>
> After many rains, rivers accretion, with remarkable washouts and spoliation of part of the peaks of these mountains, leaving them eroded, the stone is be surrounded by the air, and the soil of those places transported

A significant change-point in the erosivity time-series was detected in 1490 (red arrow in **Figure 7A**), in the central part of the LIA, either with the T-Test (Panofsky and Brier, 1958), the Worsley's likelihood ratio (Worsley, 1986) or the Standard Normal Homogeneity Test (Alexandersson, 1986). After this change-point, erosivity has become more changeable, with erosive storms tending to oscillate more, as also shown by the 11-years Gaussian filtered curve (**Figure 7A**, bold blue curve). The statistically relevant change-point provides a picture of variations in erosivity related to changes in climate patterns, with cold conditions dominating during the LIA. Hence, we note groups of annual values around and above the 98th percentile in this cold period (blue circles near the horizontal bold pink line in **Figure 7A**).

The uncertainty of hydrological information poses challenges for the analysis of historical storm data because the aggressiveness of storms evolves in complex hydrological processes, with local interactions between environmental context, climate fluctuation and human impact (Bintliff, 2002). The driving forces and actors in a close and reciprocal interaction result in cause-and-effect relationships that include feedbacks, where the erosive hazard becomes an expression of the human influence and its impact on landscape change. For instance, there is a slope effect on radiative balance and convective events (e.g., Bois et al., 2020). Thus, storm records after c. 1490 may have become more changeable due to climatic variations and human influence on slopes, resulting in less water infiltration by continuous deforestation and consequently more water available for runoff, reaching in an easier way the water lines and leading to a reduction in the time of water concentration in the basin. After the change-point, the construction of canals and ports along the Arno river led to the continuous deforestation of the timber for the consequent construction of ships, houses and other buildings (Salvestrini et al., 2010). We know that mount Morello, near Florence, already appeared deforested in the 14th century (Hofman and Perulli, 2000). Then, during the 15th and 16th centuries, the progressive deforestation of the Apennine chain and the inland reliefs accentuated the risk of seasonal runoff and flooding (Salvestrini.et al., 2017). Also in the 19th century, Targioni-Tozzetti (1852) lamented the absence of forest containment in the Grand Duchy of Tuscany for many years. Thus, natural factors related to the torrential nature of the rivers (based on the concentration of rainfall during the winter period from September to April), the steep slope of the elevation profile

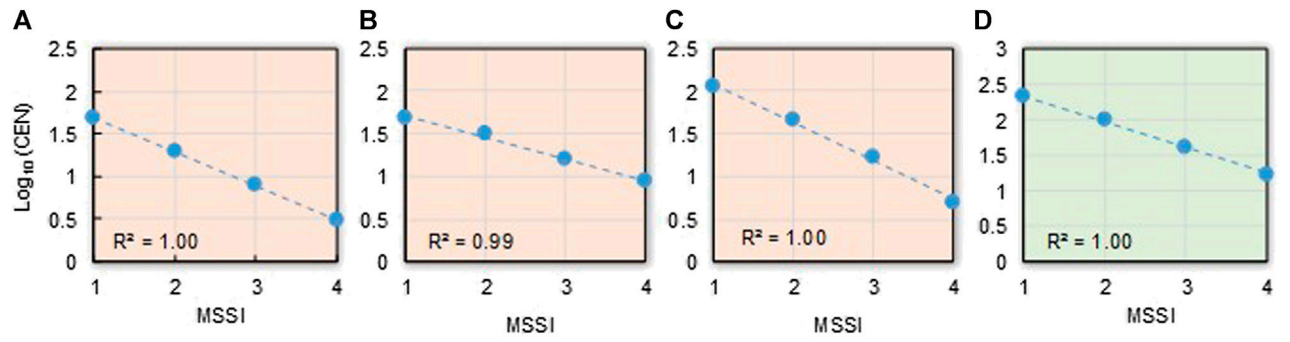


**FIGURE 5 |** Completeness of the reconstructed extreme hydrological events. Cumulative distribution of the logarithm of number of storm events vs. their Monthly Storm-Severity Index (MSSI) for sub-periods (pink colored graphs) **(A)** 1,000–1340 CE, **(B)** 1,341–1680 CE **(C)** 1,681–2019 CE, and **(D)** the entire dataset (green-coloured graph) 1,000–2019 CE for the Arno River Basin.

and the long and continuous deforestation, as well as the climatic surge triggered by solar minima, must be attributed to the clearly erosive character of the storms in the ARB until the end of the Litle Ice Age. In fact, we know that between the end of the 15th century and throughout the 16th century, the Arno River Basin was characterized by an increase in storms and floods, perhaps even favored by a worsening of the climate with the resumption of equinoctial autumn storms. Among others, extraordinary phenomena occurred in the years 1494, 1532, 1543, 1547, 1557, 1571 and 1589, characterised by a particularly strong erosive forcing of estimated 3483, 2431, 2487, 2872, 2488, 2431 and 3391 MJ mm $hm^{-2}$ $h^{-1}$ $yr^{-1}$, respectively. These events were particularly dangerous at the beginning of autumn, with concomitant tilling of soils. However, despite the awareness of the causes of the damage (deforestation, steep slopes, exploitation of the river bed) or, more simply, the fear that disasters would happen again, the Florentine administrators did not have the power to implement any protection measure because of the fragmentation of authorities and competences within the Arno River Basin: the discourse was dominated by economic considerations (timber supply, food production, protection of factories within the walls) that overlooked environmental and safety concerns (Salvestrini et al., 2010). It is precisely during this period that the Arno River Basin became most vulnerable, as it was also subject to cyclically recurrent deforestation (Ricci et al., 2017; Berti et al., 2019). It is hardly a coincidence that the climate in the central and final part of the LIA provided some injuring scenarios, with storms of unprecedented strength. In particular, the most striking group of erosive events occurred between the late 17th century and late 18th century, when we estimated erosivity values of ~1600 MJ mm $hm^{-2}$ $h^{-1}$ $yr^{-1}$ once every about four years, with estremes of ~3000 MJ mm $hm^{-2}$ $h^{-1}$ $yr^{-1}$ once every ~20 years. The two maximum estimated erosivity values for the whole series, 4892 and 3844 MJ mm $hm^{-2}$ $h^{-1}$ $yr^{-1}$, were reached in 1688 (out-of-scale value of **Figure 7A**) and 1687, respectively. These annual rates are considerable, considering that they are smoothed over the basin area, which means that even higher erosive forcing may have occurred locally in the basin. This phase has also recently been identified as erosive-prone, characterized by high runoff in the southern Carpathians (Longman et al., 2019) and flooding in most of Europe (Blöschl et al., 2020). It corresponds to the grand solar (Maunder) minimum of 1645–1715 CE (Eddy, 1976), during which sunspots became exceedingly rare with lower-than-average temperatures in Italy (**Figure 5**, bottom colored band). Maximum erosivity values occurred just with such low temperatures, with likely a greater thermal contrast between the cold fronts and the warmer Mediterranean waters, which exacerbated the thermal difference between the air and the sea, making the precipitation events more intense. An increase in high-magnitude floods was observed in central and southern Europe c. 1700, linked to the cold and dry climate of the late Maunder minimum (Mudelsee et al., 2004), a key segment of the LIA for studying decadal-scale climatic change in Europe (Luterbacher et al., 2001).

During the 20th century, erosive fluctuations began a new, albeit modest rise, with some notable values in 1938, 1966 and 2013, comparable to those of the LIA. By the onset of the 20th century, the agricultural landscape already experienced the general phenomenon of rural abandonment that become typical during the second half of the century, with a recovery of wooded areas and an urbanization of parts of the countryside to the detriment of agricultural and pasture lands (Berti.et al., 2019). Then, from 1952 onwards, the application of the mountain law led to a 15-year period of renewed fervor not only with reforestation but also with the construction of infrastructures, with the participation of peripheral bodies like municipal consortia and mountain communities (Hofman and Perulli, 2000). Summary statistics for three climatic periods (**Table 1**) show that although the mean rainfall erosivity has continued to increase from medieval times until the recent period of warming (1342–1441 MJ mm $ha^{-1}$ $h^{-1}$ $yr^{-1}$), it is during the LIA that the coefficient of variation (30%) is maximized and the 95th and 98th percentiles are particularly high (2,431 and 2760 MJ mm $ha^{-1}$ $h^{-1}$ $yr^{-1}$, respectively). The evolution of erosivity extremes (bi-decadal 98th percentiles, representing an approximation of the hydrological hazard) shows a recrudescence of the hydrological forcing, which started from the change-point year 1490 (after some peaks just prior to 1200),

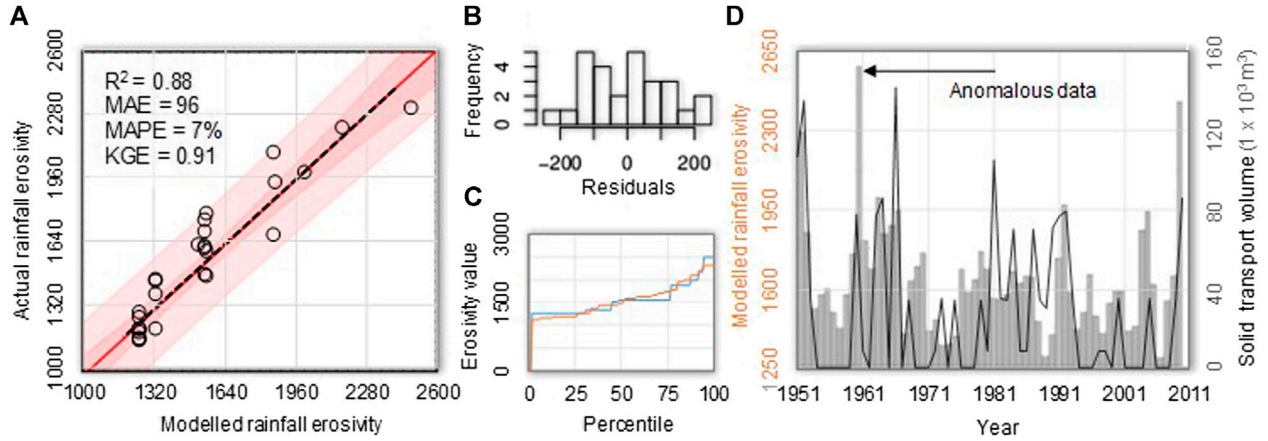


**FIGURE 6 |** Rainfall erosivity model calibration and qualitative validation in the Arno River Basin. **(A)** Scatterplot (dotted black regression line and red line of identity) of actual vs. modeled—**Eq. 2**—rainfall erosivity (MJ mm $hm^{-2}$ $h^{-1}$ $yr^{-1}$) for the 1964–1990 period, with the inner bounds showing 90% confidence limits (power pink colored area), and the outer bounds showing 95% prediction limits for new observations (light pink), **(B)** histogram of residuals, **(C)** percentiles of actual (blue curve) and modeled (orange curve) rainfall erosivity, and **(D)** coevolution of modeled annual rainfall erosivity (black line) and sand transport volumes (grey histogram) at the mouth of the Arno river in the 1951–2010 period (from Monti and Rapetti, 2011).

continued throughout the LIA until the end of the 18th century, and then manifested a statistically significant upward trend (Mann-Kendall test $p < 0.01$) (**Figure 7B**).

We have analyzed the erosivity density (ED, MJ $hm^{-2}$ $h^{-1}$), which measures the erosivity per rainfall unit and is a better indicator of the erosive hazard than rainfall erosivity (Glur et al., 2013; Diodato et al., 2019a). We addressed this issue by examining the estimated ED time-series since 1891, as it is only from this year that high-quality, well-documented, and homogeneous annual rainfall records are available for the ARB. **Figure 8A** shows that the erosive hazard has increased significantly from the end of the 19th century until 2016 (Mann-Kendall test $p < 0.05$). This means that a gradual increase in erosivity density due to extreme rainfall events has increased pressure on the landscape. Although the basin has received a fairly constant amount of precipitation from year to year (Mann-Kendall test $p > 0.05$), the aggressiveness of rainfall has become even more variable, with extreme values persisting and evolving more unexpectedly. This is in line with the results of Bezak et al. (2020), who have observed an increasing trend in the frequency of peak erosivity years in recent decades (1961–2018) in Italy, particularly in Tuscany. Though not statistically significant, the decadal trend was also positive (**Figure 8B**).

## Fingerprint of Climate Change

Evidence for an attribution to climate change of extreme erosive events associated with floods and torrential rains remains limited, partly due to the high spatial variability and unpredictability of these events in the long term. According to Cislaghi et al. (2005) and Pavan et al. (2008), the frequency of rainy days has decreased over Italy over the 19th and especially the 20th centuries, but short-duration episodes (i.e., from one to three hours) have instead enhanced the torrential character of seasonal rains. Colarieti Tosti (2014) also pointed out that in the coming decades the polar vortex is likely to undergo a phase of expansion toward southern latitudes, leading to an intensification of the hydrological cycle in the Mediterranean region. It is also expected from global model projections that the frequency of extreme rainfall events over hazard-exposed landscapes in much of Europe would increase toward the end of the 21st century (Myhre et al., 2019; Rädler et al., 2019). These results seem to reflect the observed increased hazard associated with extreme rainfall in the Mediterranean region, despite a decrease in total precipitation amounts, as claimed by Alpert et al. (2002), Paxian et al. (2015), Drobinski et al. (2018) and Bevacqua et al. (2019), but questioned by Mariani et al., (2014). De Luca and Galasso (2018) also revealed a substantial stability in the temporal and spatial behavior of intense rain events during the 20th century. These contrasting results underline that different analyses can change the perception of the type of hazard associated with hydrological processes when dissimilar metrics are used. Reconstructed rainfall erosivity in two Mediterranean fluvial basins, the Calore Basin in southern Italy (Diodato et al., 2008) and the Po Basin in northern Italy (Diodato et al., 2020c), showed similar increasing trends since the end of the LIA. If this rainfall regime continues, it could result in an increased erosive hazard affecting Mediterranean lands because erosive events occur in a more erratic way. This implies that a future increase in extreme rainfall could have serious consequences in terms of soil erosion, sudden flooding and various types of ecological disruption in the Mediterranean region (Borrelli et al., 2017). An increase of the geo-hydrological hazard due to more intense rainfall activity over the past five decades (1970–2019) is indeed recognized for hilly inland areas of central Italy (Paliaga et al., 2020). However, a sustained long-term trend, dating back to 1760, has not been observed in northern Italy, despite the marked inter-annual and inter-decadal variability of storms (Pieri et al., 2016). This underlines the need for high-resolution climate model projections to reliably predict erosive precipitation. It remains however difficult to determine how Mediterranean cyclones produce erosive trends due to

extreme rainfall events (Lionello et al., 2016). Deepening in warm waters, Mediterranean cyclones form mainly around a few centers, with a dominating area in the Gulf of Genoa (~240 km$^2$, centred on 44°10′N, 08°55 E), where a slow-moving low-pressure field (or Vb-weather pattern) can transport large amounts of rain (Hofstätter et al., 2016). While the incidence of cyclones has decreased in the Mediterranean, the increase in erosivity associated with short-term and extreme rainfall could be due to a sharp increase in convective rainfall associated with extreme events during the recent warming. Berg et al. (2013) have shown that convective rainfall is more responsive to temperature increases than frontal passages, and increasingly drives extreme erosive events. Aggressive precipitation

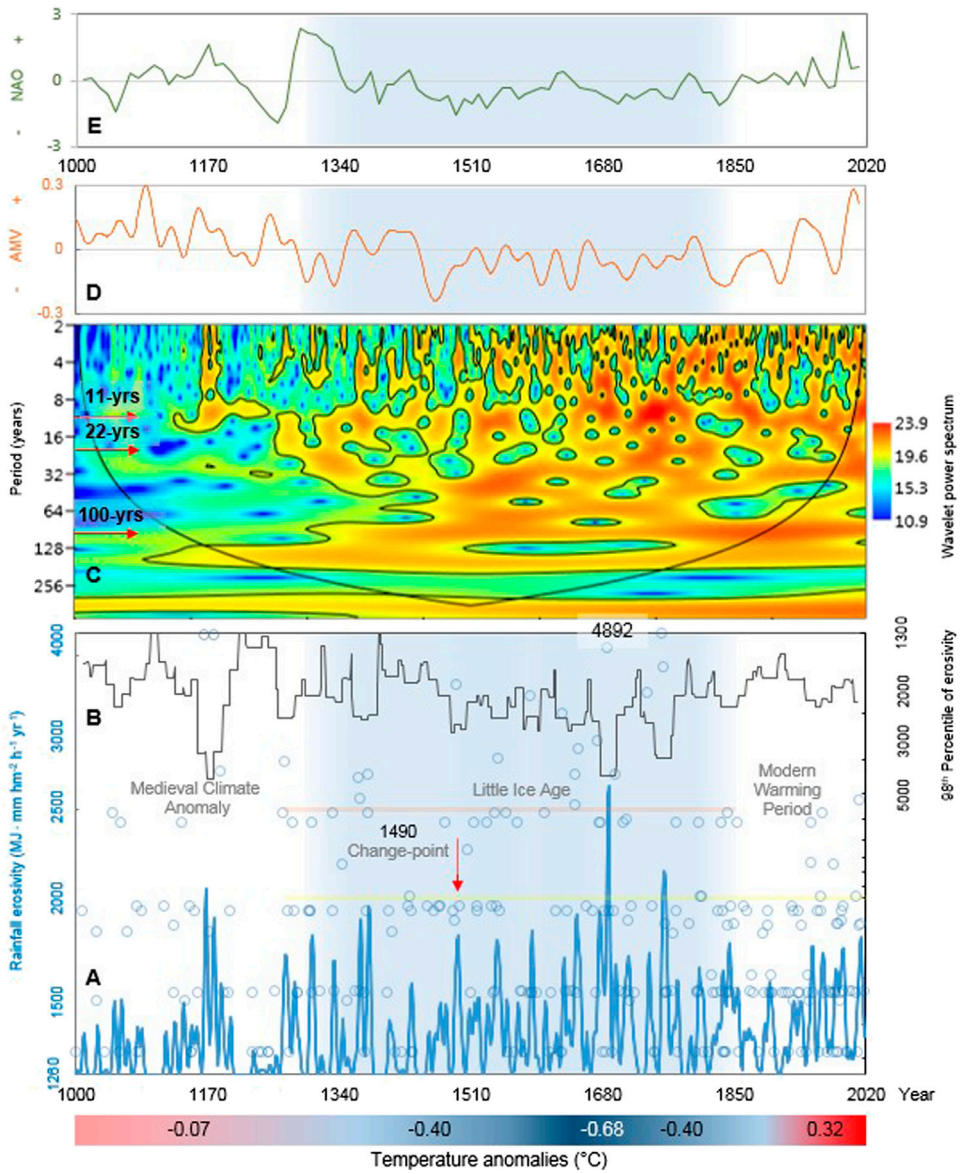


**FIGURE 7 |** Overview of erosivity and climatic patterns over the period 1000–2019 CE in the Arno River Basin. **(A)** Evolution (red arrow indicating the change-point year 1490) of estimated annual rainfall erosivity (blue circles; out-of-scale value in the year 1688) with the relative 95th and 98th percentiles (horizontal bold yellow and pink lines, respectively), and the 11-years Gaussian filtered erosivity series (bold blue curve), **(B)** decadal-scale variability of the 98th percentile of rainfall erosivity (black curve), **(C)** wavelet spectrum of the rainfall erosivity time series with bounded colors identifying 0.05 significance areas (the bell-shaped, black contour marks the limit between the reliable region and the region below the contour where the edge effects occur, a.k.a. cone of influence), **(D)** Atlantic Multidecadal Variability (AMV; Wang et al., 2017), **(E)** North Atlantic Oscillation (NAO; Hernández et al., 2020). The bottom colored band indicates mean Italian summer (June-July-August) temperature anomalies (°C) with respect to the 1961–1990 climatology (Luterbacher et al., 2016) for the Medieval Climate Anomaly, three phases of the Little Ice Age (with in dark blue the years of the Maunder minimum) and the Modern Warming Period. The Little Ice Age is identified as a light blue area across the graphs A, B, D and E. The *y*-axex in A and B are log-scales.

**TABLE 1 |** Descriptive statistics for three climatic periods of the modeled time series of rainfall erosivity. MCA: Medieval Climate Anomaly; LIA: Little Ice Age; MWP: Modern Warming Period.

| Climatic period | Mean (MJ mm ha$^{-1}$ h$^{-1}$ yr$^{-1}$) | Coefficient of variation (%) | Percentiles (MJ mm ha$^{-1}$ h$^{-1}$ yr$^{-1}$) | |
|---|---|---|---|---|
| | | | 95th | 98th |
| MCA (1,000–1249 CE) | 1,342 | 26 | 1892 | 2,431 |
| LIA (1,250–1849 CE) | 1,433 | 30 | 2,431 | 2,760 |
| MWP (1850–2019 CE) | 1,441 | 20 | 1948 | 2,342 |

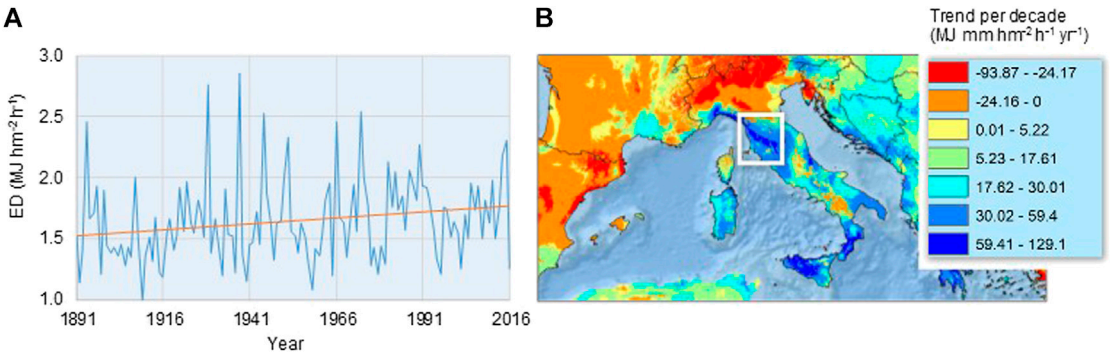


**FIGURE 8 |** Erosive susceptibility in the Arno River Basin and Tuscany **(A)** Annual evolution of erosivity density (MJ hm$^{-2}$ h$^{-1}$) from 1891 to 2016 across the Arno River Basin (blue curve) and the relative linear trend (orange line), and **(B)** rainfall erosivity trend per decade (1961–2018), with the Tuscany region (where a positive trend of erosivity is detected) highlighted by the white square (derived from Bezak et al., 2020).

is likely to become more frequent as global warming increases (AghaKouchak et al., 2018), albeit with different patterns of change in small areas without the emergence of distinct homogeneous spatial and temporal trends (Libertino et al., 2019).

## Influence of Solar and Teleconnection Cycles

The wavelet power spectrum (**Figure 7C**) reveals significant high-frequency periodicities in the erosivity time-series that tend to mirror the well-known ~11- and ~22-year sunspot cycles (with ~22-years magnetic solar cycle consisting of two ~11-year cycles with opposite polarities; Schwabe, 1843; Hale et al., 1919), and the quasi-secular (~80–100 years) Gleissberg (1958) cycle. The Sun can considerably affect the hydrological cycle through multi-scale feedbacks possibly originating complex geographical distributions of solar-related signals in hydroclimatic factors. Climate sensitivity to solar variations (magnetic activity of sunspots and the Sun's orbital dynamics), which follows a frequency-dependent solar energy transfer function (Scafetta and West, 2006), can cause regional changes in the moisture-holding capacity of the atmosphere and alter the hydrological cycle and precipitation patterns (North, 2004). In river basins in particular, the integrated nature and the inertia of river and sediment discharges may reveal solar-induced pulses that amplify precipitation signals, while the links between solar activity and precipitation may be comparably weak (e.g., Milly and Wetherald, 2002; Tomasino et al., 2004).

Our reconstructed storms (translated into rainfall erosivity data) can be considered as suitable proxies of fluvial discharges. Historical sources provide indeed a deal of evidence for the identification of hydrological extremes in the ARB, which includes the discharge of water and sediment from the river. In his *Codex Atlanticus* Leonardo da Vinci wrote for instance that "the tempest sent a sudden flood of water to submerge al the low part of this city; added to which there came a sudden rain, or rather a ruinous torrent and flood of water, sand, mood and stones, entangled with roots, and stems and fragments of various trees" (Pfister et al., 2009, p. 74). It dates to 1503 the information on "the irregularity in the flow of the Arno waters and their tendency to continuously change the river bed by transporting new sediments" (Curti, 1979, p. 40). Hints for a possible influence of solar cycles on the flood discharges of the Arno river are provided by Zanchettin et al. (2008), who found solar-type periodicities related to the magnetic activity of sunspots and suggested that Sun could be one of the drivers of hydrological processes in northern Italy. In northwest Italy (1701–2019 CE), Diodato et al. (2021) also found statistical links between rain-hazard metrics (erosivity density and return periods of erosivity peak values) and the ~22-year solar cycle together with Atlantic teleconnection patterns. These studies indicate that regional patterns of precipitation or temperature changes can be modified by large-scale climate structures (teleconnections) induced by variations in solar energy absorption in the atmosphere and ocean surface layers (Perry, 2007). In Europe, the frequency of regional precipitation oscillation peaks can be explained by persistence in atmospheric and circulation patterns

over the North Atlantic like sea-surface temperature (SST), as reflected by the Atlantic Multidecadal Oscillation (AMO) index (Willems, 2013). A possible climate mechanism governing the frequency of storm erosivity in the ARB is the Atlantic Multidecadal Variability (AMV), i.e., the change in SST in the North Atlantic. Based on terrestrial proxy records from the circum-North Atlantic region, the AMV reconstruction by Wang et al. (2017) exhibits the pronounced variability on multidecadal time-scales commonly referred to as the AMO (Kerr, 2000; Enfield et al., 2001), i.e. the internally generated component of AMV. We observe that during a warm-dominating phase of the AMV, the number of storms is significantly lower whereas during a cold-dominating phase of the AMV the number of storms is significantly higher (**Figure 7D**). In this sense, the strength of solar activity apparently modulates the connection between the AMV and the storms in the ARB.

While Sutton and Dong (2012) have identified links between the increase in mean seasonal precipitation in the Mediterranean region and the negative phases of the AMO, it is known that the AMO tends to be related to the North Atlantic Oscillation (NAO) index (Hurrell, 1995; Jones et al., 1997; Cook et al., 2019), i.e. the difference in normalised sea-level atmospheric pressures between stations near Azores (roughly 38°N) and near Iceland (roughly 65°N). Walter and Graf (2002), in particular, have shown that the AMO is negatively correlated with the NAO during its cool (negative) phases while the relationship is weak with the warm (positive) AMO phases. NAO-associated flow moisture convergence anomalies explain part of the precipitation patterns of the Mediterranean region (Seager et al., 2020). Casanueva et al. (2014) examined several Northern Hemisphere teleconnection patterns and found an increase in extreme precipitation events in the central and eastern Mediterranean regions with positive summer values of the NAO index for the period 1950–2010. In a multi-centennial perspective (1680–2019 CE), Diodato et al. (2020a) showed that substantially neutral (winter) NAO states (without a clear dominance of positive or negative phases) correspond to a decline of erosivity extremes throughout the Mediterranean. In the present basin-wide study, we observed (**Figure 7E**) a predominantly weak anti-correlation between the reconstructed erosivity time-series and the proxy-based multi-annual NAO reconstruction of Hernández et al. (2020). These studies highlight the need for a more detailed understanding of the linkages between large-scale atmospheric and oceanic oscillations and different erosivity outputs (e.g., average or extreme events), which depend on the geographic context (e.g., large regions or small river basins) and the temporal frame (e.g., seasonal or yearly) in which the hydrological response is assessed.

## CONCLUSION

Storm indicators derived from historical documentary sources offer new opportunities to develop long records of past erosivity for the detection of signals of past and present climate change. In this study, we have improved our understanding of the interannual variability of hydrological extremes in a Mediterranean fluvial basin (the Arno Basin) using a continuous time-series of rainfall erosivity, reconstructed back to 1000 CE (and over a shorter period, 1891–2016, for erosivity density). For the whole period assessed (1000–2019 CE), the main results can be summarized as follows:

1. Erosivity estimates across the ARB since 1000 CE show an alternation of stormy and calmer periods, with a change point toward the end of the 15th century (i.e., 1490).
2. The cold Little Ice Age (here, 1250–1849 CE) is characterized (especially after the change-point year) by several years with peaks of erosive storms, followed by a calmer phase (the most recent decades have seen a resumption of the erosive power of rainfall due to more intense rainfall, in parallel with an increase of erosivity density).
3. Fluctuations in the rainfall erosivity time-series indicate that changes in circulation patterns in the North Atlantic can be related to hydrological hazard in the ARB, which consists in an alternation between periods of more or less extreme erosivity in accordance with negative and positive phases of the Atlantic Multidecadal Variation.

Due to its length, the annually-resolved time-series of rainfall erosivity in the ARB, reconstructed from monthly proxy data, is unique and can be useful in discerning the fingerprint of climate change and communicating sub-regional hydrological hazards in central Mediterranean region. However, this analysis, carried out on an annual time-scale, can mask important variations that occur on even finer (e.g., monthly) time-scales. The methodology applied mainly refers to inter-annual and inter-decadal time-scales, and does not take into account daily and seasonal changes, which can have an impact on hydrology and cause damages due to loss of land. For the ARB, it has been observed that heavy erosive rainfall occurs mainly in late autumn and winter. However, the recent intensification of the hydrological regime can be attributed to convective events that occurred during the summer season, but were not captured by our model (which relies on historical sources that do not adequately describe these local phenomena) and provides a low-resolution assessment.

Continuing studies on these aspects could make important contributions in the effort to link historical and environmental research. By providing the first quantitative assessment of the long-term dynamics of erosivity extremes in the ARB, this work highlights the potential of the approach used and provides stimulus for further refinement of erosive rainfall reconstructions. The time-series of annual rainfall erosivity and erosivity density presented here are important for climate analyses on time-scales ranging from multi-decadal to centennial and even millennial lengths. It is precisely on these time-scales that changes in anthropogenic forcing are most likely to overlap with natural climate variability. The erosivity data presented can thus be used to study climate variability and extremes occurring on a sub-regional scale, which can be compared with simulations of natural and forced variability in recent times. In addition, the proposed approach could be useful for long-term planning of

environmental land-management strategies in Mediterranean areas with similar landscape features, where no direct determination of rainfall erosivity is available. By shedding light on the processes that govern long-term storm events, our results imply that environmental management can use long time-series of rainfall erosivity to estimate soil losses by water erosion occurred in past times as a basis for increasing societal resilience, informing decision making and driving further monitoring/modeling efforts. In particular, they can make policy makers aware of the urgency of reducing and controlling land degradation in the Mediterranean region.

## DATA AVAILABILITY STATEMENT

All data used in this study are freely available. Spatial patterns of mean annual rainfall erosivity over the European region (**Figure 1C**) are freely available from the ESDAC (European Soil Data Centre) dataset at https://esdac.jrc.ec.europa.eu/content/global-rainfall-erosivity. The AMV (Atlantic Multidecadal Variation) reconstruction (**Figure 7D**) was extracted from Climate Explorer of the Dutch Royal Netherlands Meteorological Institute (KNMI) at http://climexp.knmi.nl. The proxy-based NAO dataset (**Figure 7E**) is available at https://doi.pangaea.de/10.1594/PANGAEA.921916. Areal mean of annual precipitation for the Arno River Basin was retrieved from the Global Precipitation Climatology Centre (GPCC) through http://climexp.knmi.nl.

## AUTHOR CONTRIBUTIONS

ND and GB developed the original research design and collected and analyzed the historical documentary data. ND, FCL and GB wrote the article together and made the interpretations together. All authors reviewed the final manuscript.

## FUNDING

FCL was supported by the Swedish Research Council (Vetenskapsrådet, grant no. 2018-01272), and conducted the work with this article as a Pro Futura Scientia XIII Fellow funded by the Swedish Collegium for Advanced Study through Riksbankens Jubileumsfond. We thank Stockholm University publishing fund support to cover article-processing charges.

## SUPPLEMENTARY MATERIAL

The Supplementary Material for this article can be found online at: https://www.frontiersin.org/articles/10.3389/feart.2021.637973/full#supplementary-material.

## REFERENCES

Acquaotta, F., Alice, A., Bentivenga, M., Fratianni, S., and Piccarreta, M. (2019). Estimation of rainfall erosivity in Piedmont (Northwestern Italy) by using 10-minute fixed-interval rainfall data. *Időjárás* 12, 1–18. doi:10.28974/idojaras.2019.1.1

AghaKouchak, A., Huning, L. S., Chiang, F., Sadegh, M., Vahedifard, F., Mazdiyasni, O., et al. (2018). How do natural hazards cascade to cause disasters? *Nature* 561, 458–460. doi:10.1038/d41586-018-06783-6

Aiazzi, G. (1845). *Narrazioni istoriche delle più considerevoli inondazioni dell'Arno e notizie scientifiche sul medesimo*. Florence, Italy: Tipografia Piatti. [in Italian]

Alexandersson, H. (1986). A homogeneity test applied to precipitation data. *J. Climatol.* 6, 661–675. doi:10.1002/joc.3370060607

Alpert, P., Ben-Gai, T., Baharad, A., Benjamini, Y., Yekutieli, D., Colacino, M., et al. (2002). The paradoxical increase of Mediterranean extreme daily rainfall in spite of decrease in total values. *Geophys. Res. Lett.* 29, 135–154. doi:10.1029/2001GL013554

Andreolli, B., and Montanari, M. (1998). *Il bosco nel Medioevo*. Bologna, Italy: Casa Editrice Clueb. [in Italian].

Angeli, L., Costantini, R., Ferrara, R., Innocenti, L., and Costanza, L. (2007). "Stima della sensibilità all'erosione del suolo attraverso l'analisi di scenari climatici," in ASITA (Turin: proceedings of the 11th ASITA national conference), Turin, Italy, November 6–9 2007, 1–6. [in Italian].

Askew, A. J. (1991). Climate and water-a call for international action. *Hydrological Sci. J.* 36, 391–404. doi:10.1080/02626669109492521

Baldini, E., and Bedeschi, A. (2018). "Il fango, la fame, la peste. clima, carestie ed epidemie," in *Romagna nel Medioevo e in Età Moderna*. (Cesena FC, Italy: Società Editrice Il Ponte Vecchio). [in Italian].

Ballabio, C., Borrelli, P., Spinoni, J., Meusburger, K., Michaelides, S., Beguería, S., et al. (2017). Mapping monthly rainfall erosivity in Europe. *Sci. Total Environ.* 579, 1298–1315. doi:10.1016/j.scitotenv.2016.11.123

Bartolini, G., Grifoni, D., Magno, R., Torrigiani, T., and Gozzini, B. (2018). Changes in temporal distribution of precipitation in a Mediterranean area (Tuscany, Italy) 1955–2013. *Int. J. Climatol.* 38, 1366–1374. doi:10.1002/joc.5251

Bazzoffi, P., and Pellegrini, S. (1990). Caratteristiche delle piogge influenti sui processi erosivi nel periodo 1964-1990 in un ambiente della Valle dell'ERA (Toscana): evoluzione climatica e modelli previsionali. *Annali dell'Istituto Sperimentale Studio e Difesa del Suolo* 20, 161–182. [in Italian].

Becchi, I., and Paris, E. (1989). Il corso dell'arno e la sua evoluzione storica. *Acqua Aria* 6, 645–652. [in Italian].

Benvenuti, M., Bellini, C., Censini, G., Mariotti-Lippi, M., Pallecchi, P., Sagri, M., et al. (2011). "Floods, mudflows, landslides: adaptation of Etruscan-Roman communities to hydrogeological hazards in the Arno River catchment (Tuscany, Central Italy)," in *Landscapes and societies: selected cases*. (Berlin, Germany: Springer), 187–201.

Berg, P., Moseley, C., and Haerter, J. O. (2013). Strong increase in convective precipitation in response to higher temperatures. *Nat. Geosci.* 6, 181–185. doi:10.1038/ngeo1731

Berti, C., Salvatori, F., and Rome (2019). "Dinamiche e forme dell'organizzazione territoriale nella montagna Toscana dalla fine del Settecento ai giorni nostri," in *Un caso di studioL'apporto della Geografia tra rivoluzioni e riforme*. (Roman, Italy: A.Ge.I), 2659–2667. [in Italian].

Bevacqua, E., Maraun, D., Vousdoukas, M. I., Voukouvalas, E., Vrac, M., Mentaschi, L., et al. (2019). Higher probability of compound flooding from precipitation and storm surge in Europe under anthropogenic climate change. *Sci. Adv.* 5, 5531. doi:10.1126/sciadv.aaw5531

Bezak, N., Ballabio, C., Mikoš, M., Petan, S., Borrelli, P., and Panagos, P. (2020). Reconstruction of past rainfall erosivity and trend detection based on the REDES database and reanalysis rainfall. *J. Hydrol.* 590, 125372. doi:10.1016/j.jhydrol.2020.125372

Bintliff, J. (2002). Time, process and catastrophism in the study of Mediterranean alluvial history: a review. *World Archaeol.* 33, 417–435. doi:10.1080/00438240120107459

Blöschl, G., Kiss, A., Viglione, A., Barriendos, M., Böhm, O., Brázdil, R., et al. (2020). Current European flood-rich period exceptional compared

with past 500 years. *Nature* 583, 560–566. doi:10.1038/s41586-020-2478-3

Bois, B., Pauthier, B., Brillante, L., Mathieu, O., Leveque, J., Van Leeuwen, C., et al. (2020). Sensitivity of grapevine soil-water balance to rainfall spatial variability at local scale level. *Front. Environ. Sci.* 8, 110. doi:10.3389/fenvs.2020.00110

Borrelli, P., Robinson, D. A., Fleischer, L. R., Lugato, E., Ballabio, C., Alewell, C., et al. (2017). An assessment of the global impact of 21st century land use change on soil erosion. *Nat. Commun.* 8, 2013. doi:10.1038/s41467-017-02142-7

Borselli, L., Cassi, P., Sanchis, P. S., and Ungaro, F. (2004). *Studio della dinamica delle aree sorgenti primarie di sedimento nell'area pilota del Bacino di Bilancino: progetto (babi)*. Florence, Italy: Consiglio Nazionale delle Ricerche–Istituto di Ricerca per la Protezione Idrogeologica.

Boudet, H., Giordono, L., Zanocco, C., Satein, H., and Whitley, H. (2020). Event attribution and partisanship shape local discussion of climate change after extreme weather. *Nat. Clim. Change* 10, 69–76. doi:10.1038/s41558-019-0641-3

Brázdil, R., Demarée, G. R., Deutsch, M., Garnier, E., Kiss, A., Luterbacher, J., et al. (2010). European floods during the winter 1783/1784: scenarios of an extreme event during the "Little Ice age". *Theor. Appl. Climatol.* 100, 163–189. doi:10.1007/s00704-009-0170-5

Brown, L. C., and Foster, G. R. (1987). Storm erosivity using idealized intensity distributions. *Trans. ASABE* 30, 379–386. doi:10.13031/2013.3195

Capolongo, D., Diodato, N., Mannaerts, C. M., Piccarreta, M., and Strobl, R. O. (2008). Analyzing temporal changes in climate erosivity using a simplified rainfall erosivity model in Basilicata (southern Italy). *J. Hydrol.* 356, 119–130. doi:10.1016/j.jhydrol.2008.04.002

Capra, A., Porto, P., and La Spada, C. (2017). Long-term variation of rainfall erosivity in Calabria (Southern Italy). *Theor. Appl. Climatol.* 128, 141–158. doi:10.1007/s00704-015-1697-2

Cardinali, F. (1828). *Del moto e misura dell'acqua–di Leonardo da Vinci*. Bologna, Italy: Francesco Cardinali [in Italian].

Casanueva, A., Rodríguez-Puebla, C., Frías, M. D., and González-Reviriego, N. (2014). Variability of extreme precipitation over Europe and its relationships with teleconnection patterns. *Hydrol. Earth Syst. Sci.* 18, 709–725. doi:10.5194/hess-18-709-2014

Cevasco, A., Diodato, N., Revellino, P., Fiorillo, F., Grelle, G., and Guadagno, F. M. (2015). Storminess and geo-hydrological events affecting small coastal basins in a terraced Mediterranean environment. *Sci. Total Environ.* 532, 208–219. doi:10.1016/j.scitotenv.2015.06.017

Cislaghi, M., De Michele, C., Ghezzi, A., and Rosso, R. (2005). Statistical assessment of trends and oscillations in rainfall dynamics: analysis of long daily Italian series. *Atmos. Res.* 77, 188–202. doi:10.1016/j.atmosres.2004.12.014

Colarieti Tosti, C. (2014). Il clima del futuro? La chiave è nel passato. Available at: https://tinyurl.com/u5hp3w6 (Accessed November 5, 2020) [in Italian].

Cook, E. R., Kushnir, Y., Smerdon, J. E., Williams, A. P., Anchukaitis, K. J., and Wahl, E. R. (2019). A Euro-Mediterranean tree-ring reconstruction of the winter NAO index since 910 C.E. *Clim. Dyn.* 53, 1567–1580. doi:10.1007/s00382-019-04696-2

Corella, J., Valero-Garcés, B., Vicente-Serrano, S., Brauer, A., and Benito, G. (2016). Three millennia of heavy rainfalls in Western Mediterranean: frequency, seasonality and atmospheric drivers. *Sci. Rep.* 6, 38206. doi:10.1038/srep38206

Cramer, W., Guiot, J., Fader, M., Garrabou, J., Gattuso, J.-P., Iglesias, A., et al. (2018). Climate change and interconnected risks to sustainable development in the Mediterranean. *Nat. Clim. Change* 8, 972–980. doi:10.1038/s41558-018-0299-2

Curti, O. (1979). *Leonardo Da Vinci nel Museo Nazionale della Scienza e della Tecnica*. Milan, Italy: Museo "Leonardo da Vinci". [in Italian].

De Lorenzo, G. (1871). *Leonardo da Vinci e la Geologia*. Editor Zanichelli (Bologna, Italy: The Physical Object). [in Italian].

De Luca, D., and Galasso, L. (2018). Stationary and non-stationary frameworks for extreme rainfall time series in southern Italy. *Water* 10, 1477. doi:10.3390/w10101477

Diakakis, M. (2017). Flood seasonality in Greece and its comparison to seasonal distribution of flooding in selected areas across southern Europe. *J. Flood Risk Management* 10, 30–41. doi:10.1111/jfr3.12139

Diffenbaugh, N. S., and Field, C. B. (2013). Changes in ecologically critical terrestrial climate conditions. *Science* 341, 486–492. doi:10.1126/science.1237123

Diodato, N. (2004). Estimating RUSLE's rainfall factor in the part of Italy with a Mediterranean rainfall regime. *Hydrol. Earth Syst. Sci.* 8, 103–107. doi:10.5194/hess-8-103-2004

Diodato, N., and Bellocchi, G. (2012). Decadal modelling of rainfall-runoff erosivity in the Euro-Mediterranean region using extreme precipitation indices. *Glob. Planet. Change* 86–87, 79–91. doi:10.1016/j.gloplacha.2012.02.002

Diodato, N., and Bellocchi, G. (2014). Storminess and environmental change—climate forcing and responses in the Mediterranean region. Dordrecht, Netherlands: Springer.

Diodato, N., Bellocchi, G., Romano, N., and Chirico, G. B. (2011). How the aggressiveness of rainfalls in the Mediterranean lands is enhanced by climate change. *Climatic Change* 108, 591. doi:10.1007/s10584-011-0216-4

Diodato, N., Bellocchi, G., Romano, N., and Guadagno, F. M. (2016). Modelling the rainfall erosivity of the Rhone region (southeastern France) associated with climate variability and storminess. *Adv. Meteorology* 2016, 1. doi:10.1155/2016/7626505

Diodato, N., Ceccarelli, M., and Bellocchi, G. (2008). Decadal and century-long changes in the reconstruction of erosive rainfall anomalies in a Mediterranean fluvial basin. *Earth Surf. Process. Landforms* 33, 2078–2093. doi:10.1002/esp.1656

Diodato, N., Borrelli, P., Fiener, P., Bellocchi, G., and Romano, N. (2017a). Discovering historical rainfall erosivity with a parsimonious approach: a case study in Western Germany. *J. Hydrol.* 544, 1–9. doi:10.1016/j.jhydrol.2016.11.023

Diodato, N., Guerriero, L., and Bellocchi, G. (2017b). Modeling and upscaling plotscale soil erosion under Mediterranean climate variability. *Environments* 4, 58. doi:10.3390/environments4030058

Diodato, N., Borrelli, P., Panagos, P., Bellocchi, G., and Bertolin, C. (2019a). Communicating hydrological hazard-prone areas in Italy with geospatial probability maps. *Front. Environ. Sci.* 7, 193. doi:10.3389/fenvs.2019.00193

Diodato, N., Ljungqvist, F. C., and Bellocchi, G. (2019b). A millennium-long reconstruction of damaging hydrological events across Italy. *Sci. Rep.* 9, 9963. doi:10.1038/s41598-019-46207-7

Diodato, N., Gómara, I., Baronetti, A., Fratianni, S., and Bellocchi, G. (2021). Reconstruction of erosivity density in northwest Italy since 1701. *Hydrol. Sci. J., in press*.

Diodato, N., Ljungqvist, F. C., and Bellocchi, C. (2020a). Fingerprint of climate change in precipitation aggressiveness across the central Mediterranean (Italian) area. *Sci. Rep.* 10, 22062. doi:10.1038/s41598-020-78857-3

Diodato, N., Ljungqvist, F. C., and Bellocchi, G. (2020b). Historical predictability of rainfall erosivity: a reconstruction for monitoring extremes over Northern Italy (1500–2019). *Npj Clim. Atmos. Sci.* 3, 46. doi:10.1038/s41612-020-00144-9

Diodato, N., Ljungqvist, F. C., and Bellocchi, G. (2020c). Monthly storminess over the Po River Basin during the past millennium (800-2018 CE). *Environ. Res. Commun.* 2, 031004, doi:10.1088/2515-7620/ab7ee9

Drobinski, P., Silva, N. D., Panthou, G., Bastin, S., Muller, C., Ahrens, B., et al. (2018). Scaling precipitation extremes with temperature in the Mediterranean: past climate assessment and projection in anthropogenic scenarios. *Clim. Dyn.* 51, 1237–1257. doi:10.1007/s00382-016-3083-x

Duulatov, E., Chen, X., Issanova, G., Orozbaev, R., Mukanov, Y., Amanambu, A. C., et al. (2021). "Introduction and background of rainfall erosivity processes and soil erosion," in *Current and future trends of rainfall erosivity and soil erosion in Central Asia*. (Cham, Switzerland: Springer), 1–7.

Easterling, D. R., Meehl, G. A., Parmesan, C., Changnon, S. A., Karl, T. R., and Mearns, L. O. (2000). Climate extremes: observations, modeling, and impacts. *Science* 289, 2068–2074. doi:10.1126/science.289.5487.2068

Eddy, J. A. (1976). The Maunder minimum. *Science* 192, 1189–1202. doi:10.1126/science.192.4245.1189

Enfield, D. B., Mestas-Nuñez, A. M., and Trimble, P. J. (2001). The Atlantic Multidecadal Oscillation and its relation to rainfall and river flows in the continental. *U. S. Geophys. Res. Lett.* 28, 277–280. doi:10.1029/2000gl012745

Garcia-Herrera, R. F., Lionello, P., and Ulbrich, U. (2014). Preface: understanding dynamics and current developments of climate extremes in the Mediterranean region. *Nat. Hazards Earth Syst. Sci.* 14, 309–316. doi:10.5194/nhess-14-309-2014

Gascón, E., Laviola, S., Merino, A., and Miglietta, M. M. (2016). Analysis of a localized flash-flood event over the central Mediterranean. *Atmos. Res.* 182, 256–268. doi:10.1016/j.atmosres.2016.08.007

Gaume, E., Bain, V., Bernardara, P., Newinger, O., Barbuc, M., Bateman, A., et al. (2009). A compilation of data on European flash floods. *J. Hydrol.* 367, 70–78. doi:10.1016/j.jhydrol.2008.12.028

Gaume, E., Borga, M., Llasat, M. C., Maouche, S., Lang, M., Diakakis, M., et al. (2018). "Mediterranean extreme floods and flash floods,"in *The Mediterranean region under climate change*. (Marseille, France: IRD Éditions), 133–144.

Giorgini, C. (1854). *Sui fiumi nei tronchi sassosi e sull'Arno nel piano di Firenze*. Florence, Italy: Tipografia delle Murate. [in Italian].

Glaser, R., Riemann, D., Schönbein, J., Barriendos, M., Brázdil, R., Bertolin, C., et al. (2010). The variability of European floods since AD 1500. *Clim. Chan.* 101, 235–256. doi:10.1007/s10584-010-9816-7

Gleissberg, W. (1958). The eighty-year sunspot cycle. *J. Br. Astr. Assoc.* 68, 1148–1152.

Glur, L., Wirth, S., Büntgen, U., Gilli, A., Haug, G. H., Schär, C., et al. (2013). Frequent floods in the European Alps coincide with cooler periods of the past 2500 years. *Sci. Rep.* 3, 2770. doi:10.1038/srep02770

Grauso, S., Diodato, N., and Verrubbi, V. (2010). Calibrating a rainfall erosivity assessment model at regional scale in Mediterranean area. *Environ. Earth Sci.* 60, 1597–1606. doi:10.1007/s12665-009-0294-z

Guzzetti, F., Reichenbach, P., Cardinali, M., Ardizzone, F., and Galli, M. (2003). The impact of landslides in the Umbria region, central Italy. *Nat. Hazards Earth Syst. Sci.* 3 (3), 469–486. doi:10.5194/nhess-3-469-2003

Hale, G. E., Ellerman, F., Nicholson, S. B., and Joy, A. H. (1919). The magnetic polarity of sun-spots. *ApJ* 49, 153–178. doi:10.1086/142452

Harris, R. M. B., Loeffler, F., Rumm, A., Fischer, C., Horchler, P., Scholz, M., et al. (2020). Biological responses to extreme weather events are detectable but difficult to formally attribute to anthropogenic climate change. *Sci. Rep.* 10, 14067. doi:10.1038/s41598-020-70901-6

Harris, R. M. B., Beaumont, L. J., Vance, T. R., Tozer, C. R., Remenyi, T. A., Perkins-Kirkpatrick, S. E., et al. (2018). Biological responses to the press and pulse of climate trends and extreme events. *Nat. Clim. Change* 8, 579–587. doi:10.1038/s41558-018-0187-9

Hernández, A., Sánchez-López, G., Pla-Rabes, S., Comas-Bru, L., Parnell, A., Cahill, N., et al. (2020). A 2,000-year Bayesian NAO reconstruction from the Iberian Peninsula. *Sci. Rep.* 10, 14961. doi:10.1038/s41598-020-71372-5

Hofman, A. A., and Perulli, D. (2000). *La Toscana dei boschi–estratto dal volume "Attraverso le regioni forestali d'Italia*. Vallombrosa, CA: Edizioni Vallombrosa. [in Italian].

Hofstätter, M., Chimani, B., Lexer, A., and Blöschl, G. (2016). A new classification scheme of European cyclone tracks with relevance to precipitation. *Water Resour. Res.* 52, 7086–7104. doi:10.1002/2016WR019146

Hurrell, J. W. (1995). Decadal trends in the North Atlantic Oscillation: regional temperatures and precipitation. *Science* 269, 676–679. doi:10.1126/science.269.5224.676

Hussain, S. T., and Riede, F. (2020). Paleoenvironmental humanities: challenges and prospects of writing deep environmental histories. *Wires Clim. Change* 11, e667. doi:10.1002/wcc.667

Jarque, C. M., and Bera, A. K. (1981). An efficient large-sample test for normality of observations and regression residuals. *Working Pap. Econ. Econom.* 40, 20–21.

Jones, P. D., Jónsson, T., and Wheeler, D. (1997). Extension to the North Atlantic Oscillation using early instrumental pressure observations from Gibraltar and South-West Iceland, *Int. J. Climatol.* 17, 1433–1450. doi:10.1002/(SICI)1097-0088(19971115)17:13<1433::AID-JOC203>3.0.CO;2-P

Jongman, B. (2018). Effective adaptation to rising flood risk. *Nat. Commun.* 9, 1986. doi:10.1038/s41467-018-04396-1

Kaniewski, D., Marriner, N., Morhange, C., Faivre, S., Otto, T., and Van Campo, E. (2016). Solar pacing of storm surges, coastal flooding and agricultural losses in the Central Mediterranean. *Sci. Rep.* 6, 25197. doi:10.1038/srep25197

Kerr, R. A. (2000). A North Atlantic climate pacemaker for the centuries. *Science* 288, 1984–1985. doi:10.1126/science.288.5473.1984

Kiss, A. (2019). *Floods and long-term water-level changes in medieval Hungary*. Berlin, Germany: Springer.

Le Roy Ladurie, E. (1982). *Tempo di festa, tempo di carestia. Storia del clima dall'anno mille*. Turin, Italy: Einaudi. [in Italian].

Lenderink, G., and Fowler, H. J. (2017). Understanding rainfall extremes. *Nat. Clim Change* 7, 391–393. doi:10.1038/nclimate3305

Li, Y., Piao, S., Li, L. Z. X., Chen, A., Wang, X., Ciais, P., et al. (2018). Divergent hydrological response to large-scale afforestation and vegetation greening in China. *Sci. Adv.* 4, eaar4182. doi:10.1126/sciadv.aar4182

Libertino, A., Ganora, D., and Claps, P. (2019). Evidence for increasing rainfall extremes remains elusive at large spatial scales: the case of Italy. *Geophys. Res. Lett.* 46, 7437–7446. doi:10.1029/2019GL083371

Lim, K. J., Engel, B. A., Tang, Z., Muthukrishnan, S., Choi, J., and Kim, K. (2006). Effects of calibration on L-THIA GIS runoff and pollutant estimation. *J. Environ. Manage.* 78, 35–43. doi:10.1016/j.jenvman.2005.03.014

Lionello, P., Trigo, I. F., Gil, V., Liberato, M. L. R., Nissen, K. M., Pinto, J. G., et al. (2016). Objective climatology of cyclones in the Mediterranean region: a consensus view among methods with different system identification and tracking criteria. *Tellus A: Dyn. Meteorol. Oceano.* 68, 29391. doi:10.3402/tellusa.v68.29391

Llasat, M. C., Llasat-Botija, M., Prat, M. A., Porcú, F., Price, C., Mugnai, A., et al. (2010). High-impact floods and flash floods in Mediterranean countries: the FLASH preliminary database. *Adv. Geosci.* 23, 47–55. doi:10.5194/adgeo-23-47-2010

Longman, J., Veres, D., Ersek, V., Haliuc, A., and Wennrich, V. (2019). Runoff events and related rainfall variability in the Southern Carpathians during the last 2000 years. *Sci. Rep.* 9, 5334. doi:10.1038/s41598-019-41855-1

Luterbacher, J., Werner, J. P., Smerdon, J. E., Fernández-Donado, L., González-Rouco, F. J., Barriopedro, D., et al. (2016). European summer temperatures since Roman times. *Environ. Res. Lett.* 11, 024001. doi:10.1088/1748-9326/11/2/02400110.1088/1748-9326/11/2/024001

Luterbacher, J. R., Rickli, R., Xoplaki, E., Tinguely, C., Beck, C., Pfister, C., et al. (2001). The Late Maunder Minimum (1675–1715)—a key period for studying decadal scale climatic change in Europe. *Clim. Change* 49, 441–462. doi:10.1023/A:1010667524422

Mariani, L., and Diodato, N. (2014). Testing a climate erosive forcing model in the Po River Basin. *Clim. Res.* 33, 195–205. doi:10.3354/cr033195

Mariani, L., Parisi, S. G., Diodato, N., and Bellocchi, G. (2014). "Extreme rainfalls in the Mediterranean area," in *Storminess and environmental change—climate forcing and responses in the Mediterranean region*. (Dordrecht, Netherlands: Springer), 17–17.

Martin, G. J. (1967). The florence floods: 4 november 1966. *Geogr. J.* 133, 277–279.

Mazzarella, A., and Diodato, N. (2002). The alluvial events in the last two centuries at Sarno, southern Italy: their classification and power-law time-occurrence. *Theor. Appl. Climatology* 72, 75–84. doi:10.1007/s007040200014

Menduni, G. (2017). Alcune considerazioni sulla evoluzione storica recente dell'Arno fiorentino e relative narrazione. *L'Acqua* 1, 25–46. [in Italian].

Milly, P. C. D., and Wetherald, R. T. (2002). Macroscale water fluxes 3. Effects of land processes on variability of monthly river discharge. *Water Resour. Res.* 38, 17. doi:10.1029/2001WR000761

Monti, S., and Rapetti, F. (2011). Stima del trasporto torbido potenziale sul fondo del fiume Arno (Toscana) tra il 1951 e il 2010. *Atti della Società Toscana di Scienze Naturali, Memoria, Serie A* 116, 115–126. [in Italian]. doi:10.2424/ASTSN.M.2011.10

Morera, S. B., Condom, T., Crave, A., Steer, P., and Guyot, J. L. (2017). The impact of extreme El Niño events on modern sediment transport along the western Peruvian Andes (1968–2012). *Sci. Rep.* 7, 11947. doi:10.1038/s41598-017-12220-x

Morozzi, F. (1766). *Dello stato antico e moderno del Fiume Arno e delle cause e dei rimedi delle sue inondazioni*. Florence, Italy: Ristampa di Arnaldo Forni ed. [in Italian].

Mudelsee, M., Börngen, M., Tetzlaff, G., and Grünewald, U. (2004). Extreme floods in central Europe over the past 500 years: role of cyclone pathway "Zugstrasse Vb". *J. Geophys. Res.* 109, D23. doi:10.1029/2004JD005034

Mueller, V., Gray, C., and Kosec, K. (2014). Heat stress increases long-term human migration in rural Pakistan. *Nat. Clim. Chang* 4, 182–185. doi:10.1038/nclimate2103

Myhre, G., Alterskjær, K., Stjern, C. W., Hodnebrog, Ø., Marelle, L., Samset, B. H., et al. (2019). Frequency of extreme precipitation increases extensively with event rareness under global warming. *Sci. Rep.* 9, 16063. doi:10.1038/s41598-019-52277-4

Nash, J. E., and Sutcliffe, J. V. (1970). River flow forecasting through conceptual models part I–a discussion of principles. *J. Hydrol.* 10, 282–290. doi:10.1016/0022-1694(70)90255-6

North, G. R. (2004). "Recent advances in solar influences on Earth's climate," in Eos Trans. AGU Fall Meeting Supplement, Alaska, December 28, 2004 [abstract].

Outeiro, L., Úbeda, X., and Farguell, J. (2010). The impact of agriculture on solute and suspended sediment load on a Mediterranean watershed after intense rainstorms. *Earth Surf. Process. Landforms* 35, 549–560. doi:10.1002/esp.1943

Paliaga, G., Luino, F., Turconi, L., De Graff, J. V., and Faccini, F. (2020). Terraced landscapes on portofino promontory (Italy): identification, geo-hydrological hazard and management. *Water* 12, 435. doi:10.3390/w12020435

Panagos, P., Meusburger, K., Ballabio, C., Borrelli, P., Beguería, S., Klik, A., et al. (2015). Reply to the comment on "Rainfall erosivity in Europe" by Auerswald et al. *Sci. Total Environ.* 532, 853–857. doi:10.1016/j.scitotenv.2015.01.00810.1016/j.scitotenv.2015.05.020

Panofsky, H. A., and Brier, G. W. (1958). *Some applications of statistics to meteorology*. University Park, PA: University ParkMineral Industries Extension Services, College of Mineral Industries, Pennsylvania State University.

Pavan, V., Tomozeiu, R., Cacciamani, C., and Di Lorenzo, M. (2008). Daily precipitation observations over Emilia-Romagna: mean values and extremes. *Int. J. Climatol.* 28, 2065–2079. doi:10.1002/joc.1694

Pavese, M. P., Banzon, V., Colacino, M., Gregori, G. P., and Pasqua, M. (1994). "Three historical data series on floods and anomalous climatic events in Italy," in *Climate since A.D. 1500*. London and New York: Routledge, 155–170.

Paxian, A., Hertig, E., Seubert, S., Vogt, G., Jacobeit, J., and Paeth, H. (2015). Present-day and future Mediterranean precipitation extremes assessed by different statistical approaches. *Clim. Dyn.* 44, 845–860. doi:10.1007/s00382-014-2428-6

Pelucani, C., Bianca, C., and Salvestrini, F. (2017). "Leonardo: L'acqua, i diluvi, il diluvio," in *L'Acqua nemica, fiumi, inondazioni e città storiche dall'antichità al contemporaneo*. (Florence, Italy: Centro Italiano di Studi sull'Alto Medioevo), 187–204. [in Italian].

Perry, C. A. (2007). Evidence for a physical linkage between galactic cosmic rays and regional climate time series. *Adv. Space Res.* 40, 353–364. doi:10.1016/j.asr.2007.02.079

Petrucci, O., Pasqua, A. A., Diodato, N., and Bellocchi, G. (2014). *Historical climatology of storm events in the Mediterranean: a case study of damaging hydrological events in Calabria, southern Italy*. Dordrecht, Netherlands: Springer, 249–268. doi:10.1007/978-94-007-7948-8_17

Pfister, C., White, S., Mauelshagen, F., White, S., Pfister, C., and Mauelshagen, F. (2018). "General introduction: weather, climate, and human history," in *The Palgrave handbook of climate history*. (London, United Kingdom: Palgrave Macmillan), 1–17.

Pfister, L., Savenije, H. H. G., and Fenicia, F. (2009). *Leonardo da Vinci's water theory: on the origin and fate of water*. Einsham, United Kingdom: International Association of Hydrological Sciences.

Pieri, L., Rondini, D., and Ventura, F. (2016). Changes in the rainfall-streamflow regimes related to climate change in a small catchment in Northern Italy. *Theor. Appl. Climatol.* 129, 1075–1087. doi:10.1007/s00704-016-1834-6

Poirier, C., Poitevin, C., and Chaumillon, É. (2016). Comparison of estuarine sediment record with modelled rates of sediment supply from a western European catchment since 1500. *Comptes Rendus Geosci.* 348, 479–488. doi:10.1016/j.crte.2015.02.009

Pouzet, P., and Maanan, M. (2020). Climatological influences on major storm events during the last millennium along the Atlantic coast of France. *Sci. Rep.* 10, 12059. doi:10.1038/s41598-020-69069-w

Puczko, K., and Jekatierynczuk-Rudczyk, E. (2020). Extreme hydro-meteorological events influence to water quality of small rivers in urban area: a case study in northeast Poland. *Sci. Rep.* 10, 10255. doi:10.1038/s41598-020-67190-4

Rädler, A. T., Groenemeijer, P. H., Faust, E., Sausen, R., and Púčik, T. (2019). Frequency of severe thunderstorms across Europe expected to increase in the 21st century due to rising instability. *Npj Clim. Atmos. Sci.* 2, 30. doi:10.1038/s41612-019-0083-7

Raible, C. C., Messmer, M., Lehner, F., Stocker, T. F., and Blender, R. (2018). Extratropical cyclone statistics during the last millennium and the 21st century. *Clim. Past* 14, 1499–1514. doi:10.5194/cp-14-1499-2018

Reimann, L., Vafeidis, A. T., Brown, S., Hinkel, J., and Tol, R. S. J. (2018). Mediterranean UNESCO World Heritage at risk from coastal flooding and erosion due to sea-level rise. *Nat. Commun.* 9, 4161. doi:10.1038/s41467-018-06645-9

Renard, K. G., Foster, G. R., Weesies, G. A., McCool, D. K., and Yoder, D. C. (1997). *Predicting soil erosion by water: a guide to conservation planning with the Revised Universal Soil Loss Equation (RUSLE)*. Washington, DC: USDA-ARS Agriculture Handbook.

Renard, K. G., and Freimund, J. R. (1994). Using monthly precipitation data to estimate the R-factor in the revised USLE. *J. Hydrol.* 157, 287–306. doi:10.1016/0022-1694(94)90110-4

Ricci, F., Bianca, C., and Salvestrini, F. (2017). "Taglio del bosco, dilavamento delle acque e inondazioni nel bacino dell'Arno durante la seconda metà del Cinquecento," in L'acqua Nemica: fiumi, inondazioni e città storiche dall'antichità al contemporaneoFlorence: proceedings of the study conference fifty years after the flood of Florence, Florence, Italy, 08 November, 2017, 205–239. [in Italian].

Rineau, F., Malina, R., Beenaerts, N., Arnauts, N., Bardgett, R. D., Berg, M. P., et al. (2019). Towards more predictive and interdisciplinary climate change ecosystem experiments. *Nat. Clim. Chang.* 9, 809–816. doi:10.1038/s41558-019-0609-3

Rohr, C. (2013). Floods of the Upper Danube River and its tributaries and their impact on urban economies (c. 1350-1600): the examples of the towns of Krems/Stein and Wels (Austria). *Environ. Hist. Camb.* 19, 133–148. doi:10.3197/096734013X13642082568534

Rombai, L., Grifoni, S., Bianca, C., and Salvestrini, F. (2017). "L'Arno e le sue inondazioni fra Sei e Ottocento," in L'acqua Nemica: fiumi, inondazioni e città storiche dall'antichità al contemporaneo. Proceedings of the study conference fifty years after the flood of Florence, Florence, Italy, 08 November, 2017, 241–305. [in Italian].

Rossini, L. (1855). *Arno. Sue adiacenze. Sua inondazione e suoi rapporti colla pubblica salute*. Leghorn, Italy: Tipografia Fabbreschi. [in Italian].

Salvestrini, F., Bianca, C., and Salvestrini, F. (2017). "Le inondazioni a Firenze e nella valle dell'Arno dal XII al XVI secolo," in L'acqua Nemica: fiumi, inondazioni e città storiche dall'antichità al contemporaneo. Proceedings of the study conference fifty years after the flood of Florence, Florence, Italy, 08 November, 2017, 31–56. [in Italian].

Salvestrini, F. (2005). *Libera città sul fiume regale: firenze e l'Arno dall'antichità al Quattrocento*. Florence, Italy: Nardini Editore. [in Italian].

Salvestrini, F., Matheus, M., Varanini, G. M., and Pinto, G. (2010). "L'Arno e l'alluvione fiorentina del 1333," in *Le calamità ambientali nel tardo Medioevo europeo: realtà, percezioni, reazioni*. (Florence, Italy: Firenze University Press), 231–256. [in Italian].

Scafetta, N., and West, B. J. (2006). Phenomenological solar contribution to the 1900–2000 global surface warming. *Geophys. Res. Lett.* 33, L05708. doi:10.1029/2005GL025539

Schmidt, S., Alewell, C., Panagos, P., and Meusburger, K. (2016). Regionalization of monthly rainfall erosivity patterns in Switzerland. *Hydrol. Earth Syst. Sci.* 20, 4359–4373. doi:10.5194/hess-20-4359-2016

Schneider, U., Becker, A., Finger, P., Meyer-Christoffer, A., and Ziese, M. (2018). GPCC full data monthly product version 2018 at 0.5°: monthly land-surface precipitation from rain-gauges built on GTS-based and historical data. *Glob. Grid. Month. Totals* 2018, 25. doi:10.5676/DWD_GPCC/FD_M_V2018_025

Schwabe, S. H. (1843). Sonnenbeobachtungen im Jahre 1843. *Astronomische Nachrichten* 21, 233–236. [in German].

Seager, R., Liu, H., Kushnir, Y., Osborn, T. J., Simpson, I. R., Kelley, C. R., et al. (2020). Mechanisms of winter precipitation variability in the European-Mediterranean region associated with the North Atlantic Oscillation. *J. Clim.* 33, 7179–7196. doi:10.1175/JCLI-D-20-0011.1

Soens, T. (2013). Flood security in the medieval and early modern North Sea area: a question of entitlement? *Environ. Hist. Camb.* 19, 209–232. doi:10.3197/096734013X13642082568651

Sofia, G., and Nikolopoulos, E. I. (2020). Floods and rivers: a circular causality perspective. *Sci. Rep.* 10, 5175. doi:10.1038/s41598-020-61533-x

Sutton, R. T., and Dong, B. (2012). Atlantic Ocean influence on a shift in European climate in the 1990s. *Nat. Geosci.* 5, 788–792. doi:10.1038/ngeo1595

Tabari, H. (2020). Climate change impact on flood and extreme precipitation increases with water availability. *Sci. Rep.* 10, 13768. doi:10.1038/s41598-020-70816-2

Targioni-Tozzetti, G. (1852). *Notizie sulla storia delle scienze fisiche in Toscana*. Firenze, Italy: Biblioteca Palatina. [in Italian].

Thornes, J. B., (1990). *Vegetation and erosion*. Chichester, United Kingdom: Wiley & Sons, 1–24.

Tomasino, M., Zanchettin, D., and Traverso, P. (2004). Long-range forecasts of River Po discharges based on predictable solar activity and a fuzzy neural network model/Prévisions à long terme des débits du Fleuve Pô basées sur l'activité solaire prévisible et sur un modèle de réseau de neurones flou. *Hydrological Sci. J.* 49, 673–684. doi:10.1623/hysj.49.4.673.54431

Toonen, W. H. J. (2015). Flood frequency analysis and discussion of non-stationarity of the Lower Rhine flooding regime (AD 1350–2011): using discharge data, water level measurements, and historical records. *J. Hydrol.* 528, 490–502. doi:10.1016/j.jhydrol.2015.06.014

Toy, T. J., Foster, G. R., and Renard, K. G. (2002). *Soil erosion; prediction, measurement, and control*. New York, NY: John Wiley & Sons.

Van Delden, A. (2001). The synoptic setting of thunderstorms in western Europe. *Atmos. Res.* 56, 89–110. doi:10.1016/S0169-8095(00)00092-2

Viles, H., and Goudie, A. S. (2003). Interannual, decadal and multidecadal scale climatic variability and geomorphology. *Earth-Science Rev.* 61, 105–131. doi:10.1016/S0012-8252(02)00113-7

Villani, G. (1587). "Storia di Giovanni Villani cittadino fiorentino, nuovamente corretta, e alla sua vera lezione ridotta (da Baccio Valori), con riscontyro di Testi antichiFratelli," in *Con due tavole, l'una dei Capitoli, e l'altra*. Florence, Italy: Filippo, e Iacopo Giunti.

Waldman, D. (2010). *Large-scale process-oriented modelling of soil erosion by water in complex watersheds*. Available at: https://www.semanticscholar.org/paper/Large-scale-process-oriented-modelling-of-soil-by-Waldmann/19b903e68a26699d11eaaa314661e84473a28d19 (Accessed January 1, 2010).

Walter, K., and Graf, H.-F. (2002). On the changing nature of the regional connection between the North Atlantic Oscillation and sea surface temperature. *J. Geophys. Res.* 107, 7. doi:10.1029/2001JD000850

Wang, J., Yang, B., Ljungqvist, F. C., Luterbacher, J., Osborn, T. J., Briffa, K. R., et al. (2017). Internal and external forcing of multidecadal Atlantic climate variability over the past 1,200 years. *Nat. Geosci.* 10, 512–517. doi:10.1038/ngeo2962

Wei, X., Cai, S., Ni, P., and Zhan, W. (2020). Impacts of climate change and human activities on the water discharge and sediment load of the Pearl River, southern China. *Sci. Rep.* 10, 16743. doi:10.1038/s41598-020-73939-8

Wetter, O., Pfister, C., Weingartner, R., Luterbacher, J., Reist, T., and Trösch, J. (2011). The largest floods in the High Rhine basin since 1268 assessed from documentary and instrumental evidence. *Hydrological Sci. J.* 56, 733–758. doi:10.1080/02626667.2011.583613

Willems, P. (2013). Multidecadal oscillatory behaviour of rainfall extremes in Europe. *Climatic Change* 120, 931–944. doi:10.1007/s10584-013-0837-x

Wischmeier, W. H., and Smith, D. D. (1978). *Predicting rainfall erosion losses: a guide to conservation planning*. Washington, DC: U.S. Department of Agriculture.

Worsley, K. J. (1986). Confidence regions and tests for a change-point in a sequence of exponential family random variables. *Biometrika* 73, 91–104. doi:10.1093/biomet/73.1.91

Wuepper, D., Borrelli, P., and Finger, R. (2020). Countries and the global rate of soil erosion. *Nat. Sustain.* 3, 51–55. doi:10.1038/s41893-019-0438-4

Zanchettin, D., Rubino, A., Traverso, P., and Tomasino, M. (2008). Impact of variations in solar activity on hydrological decadal patterns in northern Italy. *J. Geophys. Res.* 113, D12102. doi:10.1029/2007JD009157

Zhang, X., Zwiers, F. W., Li, G., Wan, H., and Cannon, A. J. (2017). Complexity in estimating past and future extreme short-duration rainfall. *Nat. Geosci.* 10, 255–259. doi:10.1038/ngeo2911

Zittis, G., Hadjinicolaou, P., Klangidou, M., Proestos, Y., and Lelieveld, J. (2019). A multi-model, multi-scenario, and multi-domain analysis of regional climate projections for the Mediterranean. *Reg. Environ. Change* 19, 2621–2635. doi:10.1007/s10113-019-01565-w

Zscheischler, J., Martius, O., Westra, S., Bevacqua, E., Raymond, C., Horton, R. M., et al. (2020). A typology of compound weather and climate events. *Nat. Rev. Earth. Environ.* 1, 333–347. doi:10.1038/s43017-020-0060-z

**Conflict of Interest:** The authors declare that the research was conducted in the absence of any commercial or financial relationships that could be construed as a potential conflict of interest.